DESIGN AND MECHANICAL CHARACTERIZATION OF A MAGNETOCALORIC PUMP

by

Erick O. Bermudez Torres

A thesis submitted in partial fulfillment of the requirements for the degree of

MASTER OF SCIENCES
in
MECHANICAL ENGINEERING

UNIVERSITY OF PUERTO RICO
MAYAGÜEZ CAMPUS
2007

Approved by:

_____   _____
Oscar Perales, PhD   Date
Member, Graduate Committee

_____   _____
Nellore Venkataraman, PhD   Date
Member, Graduate Committee

_____   _____
Gustavo Gutierrez, PhD   Date
President, Graduate Committee

_____   _____
Sonia Bartolomei, PhD   Date
Representative of Graduate Studies

_____   _____
Paul Sundaram, PhD   Date
Chairperson of the Department

ABSTRACT

In this thesis, a Magnetocaloric Pump (MCP) able to convert heat into power by using the magnetocaloric effect is studied and designed. The actual pressure head is compared with the simplified Bernoulli equation for magnetic fluids and some important design parameters are identified and clarified. Two $Mn_x Zn_{1-x} Fe_2 O_4$ (a water-based and a hydrocarbon-base) ferrofluids are compared in order to analyze their magnetocaloric effect. The synthesis procedure is improved and ferrites production is found to be scalable. For the produced water-based ferrofluid, a chemical co-precipitation method and a double layer surfactant technique are employed in the production of the ferrofluids. The effect of the saturation magnetization Ms and the Curie temperature in the pump performance as well as the heating source position inside the induced magnetic field of approximately 0.5 Tesla are tested. Optimum operational conditions were established and an efficient ferrofluid suitable for electronic cooling applications is selected according to the maximum pressure head reached by the pump.

RESÚMEN

La siguiente tesis se basa en el diseño y estudio de una Bomba Magnetocalórica (MCP) capaz de convertir calor en potencia utilizando el efecto magnetocalórico. El cabezal de presión obtenido es comparado con la ecuación de Bernoulli simplificada aplicable a fluidos magnéticos y ciertos parametros críticos no icluidos en dicha ecuación fueron identificados y clarificados. Dos ferrofluidos de $Mn_xZn_{1-x}Fe_2O_4$ (uno suspendido en base de agua y otro suspendido en un hidrocarburo) y dos ferrofluidos de Fe_3O_4 (uno suspendido en una base de agua y otro suspendido en aceite) son comparados para analizar su efecto en la funcionalidad de la bomba. Se logró mejorar significativamente el proceso de síntesis empleado para la fabricación de las ferritas y los de ferrofluidos, facilitando así su producción en masa. Para la fabricación de los fluidos fueron empleados el metodo de co-precipitación y la técnica de doble recubrimiento de surfactante. Se investigó el efecto de la magnetización de saturación, la temperatura de Curie y la posición de la fuente de calor dentro del campo de inducción magnética en el sistema diseñado. De acuerdo al máximo cabezal de presión obtenido, se establecieron las condiciones operacionales idóneas y se seleccionó el ferrofluido adecuado para ser empleado en aplicaciones relacionadas al enfriamiento de equipos electrónicos.

DEDICATION

To my daughter Noelia and my wife Linda. To my father Jorge and my mother Dora, my brother Jorge Esteban and my sisters Glenda and Evelyn. Thanks for being all my strength and inspiration. I love you all

ACKNOWLEDGEMENTS

CONTENTS

LIST OF FIGURES

LIST OF TABLES

LIST OF NOMENCLATURE

Cl	Chloride
Cp	Specific heat
D,d	Diameter
f	Friction factor
Fe	Iron
FTIR	Fast Transform Infrared
G	Gauss
g	Gravitational constant
H	Applied magnetic field
h	Pressure head
H_c	Coercivity
HRTEM	High Resolution Transmission Electron Microscope
ID	Internal diameter
K	Pyromagnetic coefficient
k	Scherer's constant
k_B	Boltzmann constant
L	Length
L_e	Equivalent length
M	Magnetization
MCP	Magnetocaloric Pump
M_d	Domain magnetization
MHD	Magnetohydrodynamic
Mn	Manganese
M_r	Magnetization of remanence
M_s	Saturation magnetization
Na	Sodium
O	Oxygen
OD	Outside diameter
P	Pressure

PVC	Polyvinyl Chloride
$\dot{q}$	Power
Re	Reynolds number
SQUID	Super Quantum Interference Device
T	Temperature
t	Time
T_C	Curie Temperature
TEM	Transmission Electron Microscope
V	Volume
v	Velocity
x	Atomic ratio
XRD	X-ray diffraction
Zn	Zinc
β	Integral breadth of reflection
χ	Magnetic susceptibility
ϕ	Volumetric fraction
η	Friction
λ	Wavelength of radiation
μ	Viscosity
μ_0	Permeability of the free space
θ	Angle
ρ	Density

1. INTRODUCTION

Certain magnetic materials tend to loose magnetization when they heat up and become magnetic again when they cool down. The phenomenon is known as magnetocaloric effect. In general terms, for a given material, the larger the change in magnetic field, the larger the magnetocaloric effect [1]. This principle was first proposed in 1918 by Piere Weiss and Auguste Picard. However, Nicolai Tesla and Tomas Edison noticed its further application but unsuccessfully attempted to run heat engines to produce power more than twenty-five years earlier. More recently, a new idea was introduced in which the magnetic conversion of heat to work could be made efficient at normal or elevated temperatures. Direct and efficient conversion of heat to work with no mechanical moving parts was shown to be possible in theory [1]. A promising application of this principle is the use of magnetic fluids with large change in magnetization as they are heated up; although, the most widely used commercially available magnetic fluids like magnetite ferrofluids do not satisfy these requirements. Therefore, the development and synthesis of special temperature sensitive magnetic nanoparticles for ferrofluids is of great interest. In this field, Mn-Zn ferrites have been shown to be the most promising candidate of the discussed application [4, 5].

The present work is focused on the design of a system using the magnetocaloric effect to convert heat into useful work and the development of suitable Mn-Zn ferrofluids valuable for magnetocaloric energy conversion.

1

1.1 Motivation

Through the years, failure for over heating and collapses of critical components due to vibrations has been a big issue in the electronic industry. The proposed device may use the undesire heat generated in electronic components to run a pumping device, at the same time it removes heat from the system. In addition, the possibility of pump a high thermal conductivity fluid using no-moving mechanical parts represents an opportunity to reduce mechanisms of fatigue and vibrations breakdown. However, there are many ignored parameters when the magnetocaloric effect is being put in practice that could represent significant errors when compared with the theoretical approaches: heat source location, magnetic induction effective area, hydraulic losses, etc.

Principles and technologies developed in this study would impact on the thermal management of engineering systems working at near ambient temperatures, such as electronic devices.

1.2 Objectives and Tasks

- Design and fabricate a magnetocaloric pump prototype (MCP) to demonstrate the concept of magnetocaloric energy conversion.
- Parameterize the system in order to provide recommendations for its optimal operational conditions to make it suitable for electronic cooling applications.
- Define optimum synthesis conditions for $Mn_x Zn_{1-x} Fe_2 O_4$ ferrites nanoparticles (x=0.7) by using the co-precipitation method.
- Disperse and stabilize the ferrite nanoparticles in a water-based solution.

▪ Characterize the Mn-Zn ferrite as well as the ferrofluids.

1.3 Background

1.3.1 Magnetism

Magnetism is a phenomenon through which materials exert an attractive or repulsive force on other materials. The contribution to net magnetic moment is originated principally by two sources: one is related to the orbital motion and the other one is attributed to the spin motion. The Bohr theory of magnetism states that an electron which orbits around the nucleus of an atom originates the magnetic behavior of matter. An electron could be considered a small current loop, producing a very small magnetic field and having magnetic moment along its axis of rotation as schematically illustrated in figure 1[2]. However, in 1925 Goudsmit and Uhlembek [3] introduced the concept of electron spin, which better explains the origin of magnetism. Spin is the movement of the electron around its axis, which also contributes to the magnetic moment in the atom. Therefore, each electron in an atom could represent a small magnet having permanent orbital and spin magnetic moments [3].
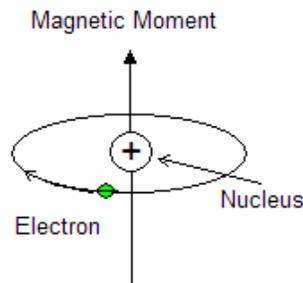
Figure 1: Schematic of an electron moving in an orbit.

One of the fundamental concepts in magnetism is the magnetic field. A field is generated in a volume of space when there is a change in energy of that volume. The force

produced by the energy gradient can be detected by the acceleration of an electric charge moving in the field, by the force on a current-carrying conductor, or by the torque on a magnetic dipole [2]. In general terms, a magnetic field is produced when an electric charge is in motion. [2, 3].

Magnetic behavior of materials

The particular response of the materials in the presence of a magnetic field determines its classification. Then, a material could be ferromagnetic, antiferromagnetic, ferrimagnetic, paramagnetic, diamagnetic or superparamagnetic, depending on the net magnetic moment of its atoms [3]

In the case of ferromagnetic materials, the dipolar interactions promote a parallel alignment of the magnetic dipole vectors, resulting in a material that has a net magnetization in the absence of an external magnetic field [3]. Figure 2 illustrates schematically the atomic dipole configuration for a ferromagnetic material. This classification includes nickel, iron, cobalt and some rare earths.

On the other hand, the antiferromagnetic materials do not exhibit any net magnetization even in the presence of an external magnetic field; because the dipoles of adjacent atoms are aligned in opposite directions (figure 2(b)). Manganese and Chromium presents an antiferromagnetic behavior at room temperature.

In ferrimagnetic materials, the dipoles of the adjacent atoms align in opposite directions but the magnitude or the number of moments pointing in one direction is different than the ones pointing in the opposite direction; creating a considerable net magnetization in the absence of a magnetic field (fig 2 (c)). They have a lower magnetization when compared with the ferromagnetic materials due to the effect of these opposite dipole moments. Ferrite and magnetite shows this behavior under certain crystal size and temperatures conditions.
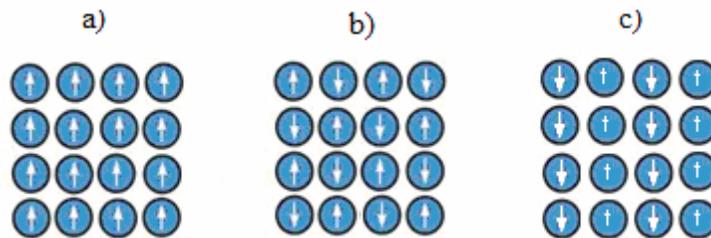
Figure 2: Magnetic dipoles array for a) ferromagnetic, b) antiferromagnetic, c) ferrimagnetic materials in the absence of an external magnetic field. The arrows represent atomic dipoles moments.

The materials whose atomics moments tend to be aligned under the presence of an external magnetic field and misaligned when this field is removed are called paramagnetic materials [3]. The difference between them and the diamagnetic ones raises only in the very small magnitude and negative magnetic effect the diamagnetic materials have. Figures 3 and 4 presents an schematic of atomic magnetic dipoles with and without the presence of a magnetic field for paramagnetic and diamagnetic materials (The arrows represent atomic dipoles moments). Among the paramagnetic materials are found the sodium, aluminum and calcium while copper, gold and silver presents a diamagnetic behavior.
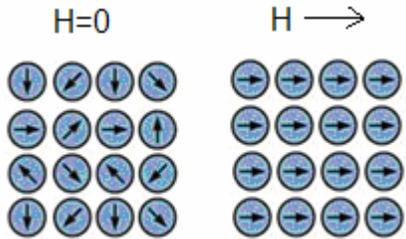
Figure 3: Magnetic dipoles configuration for a paramagnetic material
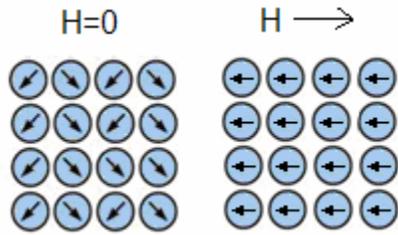
Figure 4: Magnetic dipoles configuration for a diamagnetic material

Finally, a superparamagnetic material exhibits both, ferromagnetic and paramagnetic behavior under some particular conditions and occurs only when the material is composed of very small crystals (generally in the order of 1nm to 20 nm). Such materials exhibit ferromagnetic or ferrimagnetic properties in bulk, but will present a paramagnetic behavior when the material reaches the Curie temperature and the thermal energy is enough to misalign the magnetic dipoles and the resulting fluctuations in the direction of magnetization causes the induced magnetization go to zero. Magnetite and ferrites are two examples of superparamagnetic materials and it has been found to have remarkable applications in ferrofluids, sensors and bio-medical applications [4,5]

Typical magnetization curves describing the magnetic behavior of materials are presented in figure 5. Such curve describes the change in magnetization or magnetic flux of the material with respect to the applied field. H_c is the coercivity defined as the magnetic

field required to demagnetize the material. M_s is the saturation magnetization (maximum magnetization value obtained under the influence of an induced external magnetic field). At this point, it is assumed that all the magnetic dipoles are oriented in the same direction of the induced magnetic field. The strength of the response to an induced magnetic field $\left(\dfrac{\partial M}{\partial H}\right)$ is known as the magnetic susceptibility (χ), and the remanence magnetization M_r, represents the ability of a material to maintain its magnetic dipoles aligned even when the external magnetic field has been removed.
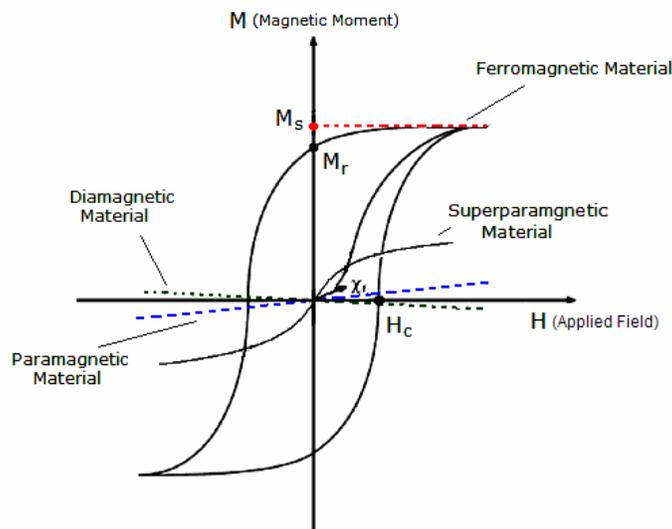
Figure 5: M-H hysteresis loop and magnetic behavior for different materials [5].

1.3.2 The Curie Temperature

The temperature at which a materials loose it magnetization and begin to behave as paramagnetic is called the Curie temperature. The Curie temperature provides an estimation of the amount of energy required to break up the long-range domain ordering

in the material. A typical curve of the domain magnetization as function of temperature is shown in figure 6.
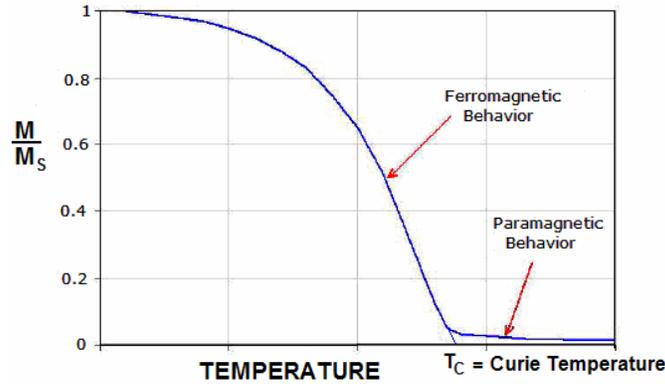
Figure 6: Temperature effect in magnetization

Close to the Curie temperature, the magnetization effect with respect to the temperature could be assumed to have a linear behavior [1, 6]. Therefore, the magnetization can be found as follows:

$$M = K(T_c - T)$$

(1.1)

Where K is known as the pyromagnetic coefficient $\left(K = -\dfrac{\partial M}{\partial T} \right)$

Thus, the Curie temperature can be obtained performing an extrapolation from the linear section of the curve of the domain magnetization until reach the temperature axis (see figure 6). However, a better approximation can be obtained by setting the maximum point of curvature from the graph and calculating the second derivative of the magnetization

8

with respect to the temperature $\left(\dfrac{\partial^2 M}{\partial T^2}\right)$ where the maximum value of the second derivative corresponds to the maximum curvature point [7, 8].

1.3.3 Ferrites

The most important ferrimagnets are the materials known as ferrites. Ferrites are ferrimagnetic oxides and therefore are electrically insulating. Ferrites are widely used in high-frequency applications, because an AC field does not introduce undesirable eddy currents in an insulating material [1, 3]. Ferrites have two different symmetries, which are determined by the size and charge of the metal ions that balance the charge of the oxygen ions, and their relative amounts.

Cubic ferrites

The cubic ferrite has the general formula $MO \cdot Fe_2O_3$ where M is a divalent metal ion. These ferrites crystallize in the spinel lattice. The spinel lattice is composed of a close-packed oxygen arrangement in which 32 oxygen ions for the unit cell (smallest reappearing unit in the crystal network). These ions are packed in a face centered cubic (FCC) arrangements leaving two kinds of spaces between anions; tetrahedrally coordinated sites (A), surrounded by four nearest oxygen atoms, and octahedrally coordinated sites (B), surrounded by six nearest neighbor oxygen atoms. These are illustrated in figure 7. [9]
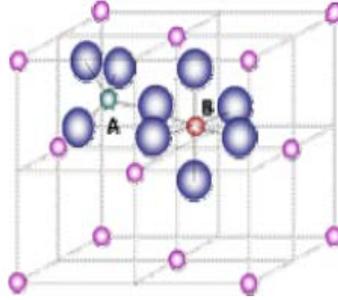
Figure 7: Schematic of two subcells of a unit cell of the spinel structure [2]

The location of ions either in A or B sites depends fundamentally on the ion and lattices sizes. In addition, it has been observed to depend on temperature and the orbital reference for specific coordination.

The cubic ferrite is easily magnetized and demagnetized, having high permeability and saturation magnetization and low electrical conductivity [5,6].

Hexagonal ferrites

Hexagonal ferrites are widely used as permanent magnets and are characterized by possessing a high coercivity []. Their general formula is $MO \cdot 6Fe_2O_3$ where M could be Ba, Sr or Pb. The hexagonal ferrite lattice is similar to the spinel structure, with the oxygen ions closely packed, but some layers include metal ions, which have practically the same ionic radii as the oxygen ions. This lattice has three different sites occupied by metals: tetrahedral, octahedral, and trigonal bi pyramid (surrounded by five oxygen ions) [9].

Ferrites are characterized by square-shaped hysteresis loops, which originate from their large magnetocrystalline anisotropy. Adittionally, they have short relaxation times, minimal mechanical strength and low magnetostriction [9].

1.3.4 Magnetic fluids

Ferrofluids or magnetic fluids are stable colloidal suspensions of magnetic particles dispersed in a liquid carrier. Particle sizes generally range from 5 to 30 nm and the volumetric loading from 5% to 10%. In a stable magnetic fluid, the size of the magnetic particles must be well controlled not only to tune the magnetic behavior within the single domain limits but also to keep non-agglomerated particles in suspension even during exposure to strong magnetic fields. Particles agglomeration and subsequent settling can be avoided by using a surfactant or other type of coating [4]. The coating agent must be matched to the carrier type and it must overcome the Van der Waals and magnetic forces in order to prevent agglomeration and further precipitation of the nanoparticles. A schematic of a ferrofluid composition is presented in figure 8.
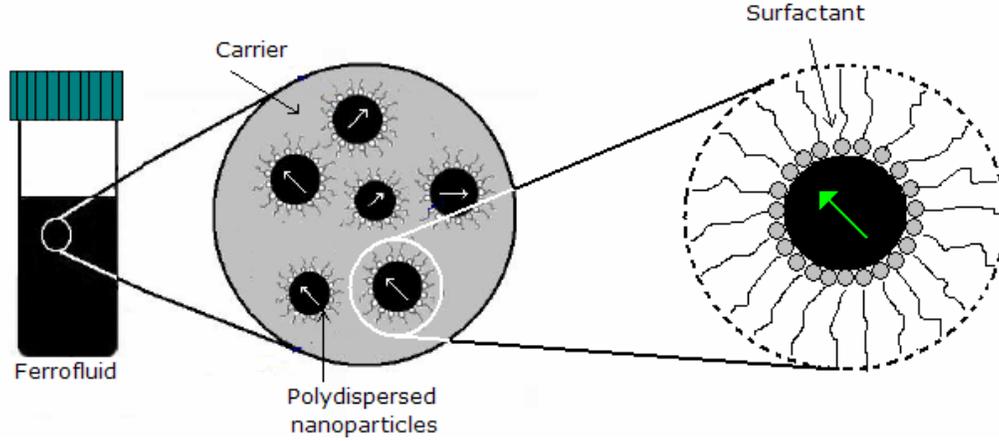
Figure 8: Ferrofluid composition schematic

1.3.5 Stability of suspension

A crucial factor in ferrofluid preparation is its colloidal stability. Stability is determined fundamentally by thermal energy ($k_B T$), where k_B is the Boltzmann's constant $\left(1.38 X 10^{-23} \frac{Nm}{K}\right)$; magnetic energy $\mu_0 HMV$, where $\mu_0 H$ is the magnetic induction (Tesla), M is the magnetization intensity and V represents the volume of a spherical particle ($V=d^3/6$) ; and gravitational energy $\Delta\rho V dg$ where $\Delta\rho$ is the difference between the powder and the fluid densities and g is the gravitational constant [1].

Stability against magnetic agglomeration

A typical ferrofluid contains approximately 10^{23} particles/m^3 [1], and collisions between particles are common. Each particle is permanently magnetized causing clustering and eventual instability in a magnetic filed gradient. However, this phenomenon could be

avoided by using suitable dispersants. The amount of energy required to separate two particles is called dipole-dipole contact energy:

$$E_{dd} = \frac{1}{12}\mu_0 M^2 V \qquad (1.2)$$

Where $\mu_0 = 4\pi \ X \ 10^{-7} \ Hm$ is the permeability of the free space. When higher to the dipole-dipole contact energy, thermal agitation can broke such agglomeration effect according to:

$$\frac{12k_B T}{\mu_0 M^2 V} \geq 1 \qquad (1.3)$$

Thus, the particle size must obey:

$$d \leq \left(\frac{72k_B T}{\pi \mu_0 M^2} \right)^{1/3} \qquad (1.4)$$

However, in such cases where the dipole-dipole interactions are considerably weak [1], agglomeration against magnetic interaction between particles can be neglected.

Stability in a magnetic field gradient

The nanoparticles are attracted to the higher-intensity region when they are placed in a magnetic field gradient; thermal agitation counteracts the field force and provides random motions that allow the dispersion of particles to be uniformly in the fluid. Stability against segregation is then given by the ratio of the thermal energy to the magnetic energy:

$$\frac{k_B T}{\mu_0 H M V} \geq 1 \qquad (1.5)$$

Therefore, the maximum particle size is determined by:

$$d \leq \left(\frac{6 k_B T}{\pi \mu_0 HM} \right)^{1/3} \qquad (1.6)$$

Stability against settling in a gravitational field

Gravity force is always trying to sediment particles against thermal agitation. This is similar to the effect of the magnetic forces in the fluid at any point of a single particle. The ratio between gravitational and magnetic energy states the mechanism to avoid segregation as follows:

$$\frac{\Delta \rho d g}{\mu_0 HM} << 1 \qquad (1.7)$$

For stability condition, the diameter of the particles must be the smallest diameter obtained from equations 1.3, 1.4, 1.6 and 1.7. However, the smallest the particles, the more difficult to align and magnetize them.

1.3.6 Ferrites by the co-precipitation method

The synthesis of $Mn_x Zn_{1-x} Fe_2 O_4$ ferrites is performed via the co-precipitation method as reported by Perales, O. et. al, 2003; the co-precipitation method is the most popular method used today among the size-reduction and microbial synthesis methods [5]. In the co-precipitation method, a solution containing Fe(III) and a divalent metal cation M(II) at suitable mole ratios is mixed with a hot alkaline solution. The hydrolysis reaction leads to the formation of a mixed paramagnetic Fe-M hydroxide, which undergoes dehydration and atomic rearrangement conductive to stoichiometric ferrite structure without the need of further annealing according to:

$$2Fe^{+3} + M^{+2} + 8OH^- \rightarrow Fe_2M(OH)_8 \rightarrow MFe_2O_4 + 4H_2O \qquad (1.8)$$
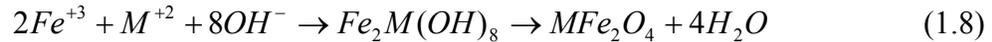
In this work, suitable weights of Zn(II), Mn(II) and Fe(III) salts are employed to get different stoichiometric compositions. Therefore, for a certain amount of Fe(III) employed, the amount of Mn(II) and Zn(II) is fixed. The ferrite nanoparticles composition is then obtained from the ratio of Mn(II) to the complete metal cation Mn(II) plus Zn(II) as follows:

$$x = \frac{Mn}{Mn + Zn} \qquad (1.9)$$

Initial molar portion of the co-precipitating agent does not maintain the stoichiometric relation and an excess of OH^- becomes necessary. The amount of the base and its concentration are determined experimentally [9, 10]

The nucleation rate tends to be high at the beginning of the synthesis whereas the excess of OH^- ions provide a net negative surface charge to the nuclei limiting their further growth and agglomeration. Under such conditions, polydisperse particles are commonly obtained [5, 10].

1.3.7 Magnetocaloric effect and the Magnetocaloric Pump

The concept of magnetocaloric power systems using the temperature dependence of the magnetic moment to convert heat into useful work was first proposed by Rosenweig [1],

who showed that direct and efficient energy conversion of heat work with no moving parts is possible.

A Magnetocaloric Pump (MCP) provides a simple mean of pumping fluid using only external magnetic and thermal fields. It uses a magnetic fluid that when exposed to a temperature gradient and a uniform magnetic field tends to loose it magnetization as it approaches the Curie temperature (temperature tends to misalign magnetic dipoles with respect to the applied magnetic field) [2]. Therefore, a heated magnetic fluid can be displaced by the colder fluid that has not yet been exposed to the heating source (see figure 9).
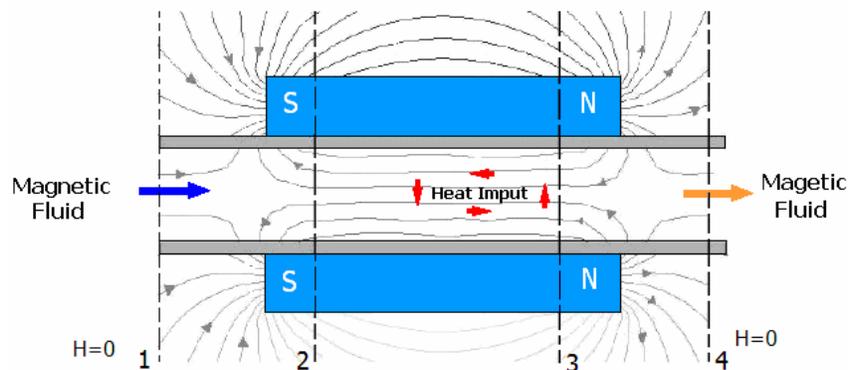
Figure 9: Ferrofluid exposed to a heating source and a uniform magnetic field

A temperature gradient induces a magnetization gradient on the magnetic fluid and the pressure gradient generated due to the change in the fluid magnetization is called *magnetocaloric effect.* Hence, it is possible to obtain a pressure gradient with no moving mechanical parts involved other that a column of magnetic fluid exposed to an external magnetic field. High Curie temperature will result in a reduction of ΔM and consequently in a reduction in the pressure gradient; however, if the Curie temperature is

far above the operational temperature of the system, the change in magnetization would be negligible (see figure 10).
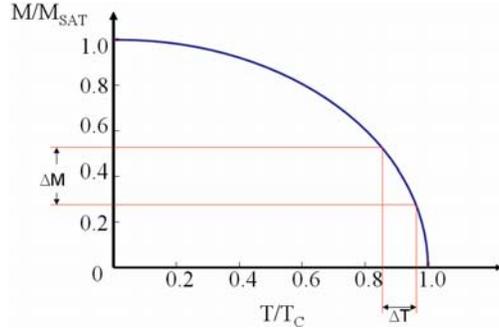
Figure 10: Magnetocaloric effect

Most commercial grade magnetic fluids use magnetite nanoparticles having a Curie temperature over 500 ℃ [1], too high for electronic cooling applications.

Then, obtain a ferrofluid with a Curie temperature near 100 ℃ is crucial for this investigation.

1.3.8 The Ferrohydrodynamic Bernoulli equation

Under steady state conditions and assuming the fluid to be incompressible and inviscid; irrotational flow and temperature independent of magnetization the Bernoulli equation for magnetic fluids can be written as:

$$P^* + \frac{1}{2}\rho V^2 + \rho g h - \mu_0 \bar{M} H = Const. \tag{1.10}$$

Where $\bar{M}$ is the field-average magnetization defined as:

$$\overline{M} = \frac{1}{H} \int_0^H M dH \qquad (1.11)$$

Then, neglecting potential energy and by assuming constant gravitational force and constant cross-sectional pipe equation 1.10 reduces to:

$$0 = -\nabla P^* + \mu_0 M \nabla H \qquad (1.12)$$

And the pressure between section 1 and 2 (see fig. 8) can be written as follows:

$$P_1^* = P_2^* - \mu_0 \overline{M} H \big|_2 \qquad (1.13)$$

Similarly section between 3 and 4

$$P_3^* - \mu_0 \overline{M} H \big|_3 = P_4^* \qquad (1.14)$$

While in sections 1 and 4 (no external magnetic field) the pressure effect reduces to:

$$P_{1,4}^* = P(\rho, T) \big|_{1,4} \qquad (1.15)$$

Since the magnetic field between sections 2 and 3 is considered to be uniform due to the temperature effect reduces that magnetic effect, $\nabla H = 0$ and consequently

$$P_2^* = P_3^* \qquad (1.16)$$

Thus substituting (1.14) in to (1.13) the pressure gradient between section 1 and 4 remains:

18

$$P_1 + \mu_0 H \left. \overline{M} \right|_2 - \mu_0 H \left. \overline{M} \right|_3 = P_4$$

$$P_4 - P_1 = \mu_0 H \left(\overline{M} \, T_2 - \overline{M} \, T_3 \right)$$

$$\Delta P = \mu_0 H \Delta \overline{M} \qquad (1.17)$$

This way the possibility to transform thermal energy into mechanical energy has been demonstrated theoretically. Equation 1.17 is known as the simplified Bernoulli equation and it will be used for the magnetocaloric pump analysis.

2. REVIEW OF LITERATURE

2.1 Contribution of this research

This research contributes to a better understanding of parameters that are important in the design of a magnetocaloric pump and its application in electronic cooling.

The proposed magnetocaloric pump will be evaluated varying the induced magnetic field magnitudes as well as the temperature gradients. The optimum heating source location with respect to the magnetic field is determined and compared with the results obtained by Shuchi et al. [11]. The synthesized nanoparticles and ferrofluid is performed based on the work done by Perales, and Almurugan ([10],[6]) and the results is compared based no only on saturation magnetization but with respect to the pyromagnetic coefficient and the

produced pressure gradient as well. The synthesis procedure is improved in order to scale the process for the ferrofluid mass production. In addition, the nanoparticles and the different ferrofluids are characterized via X-ray diffraction and magnetic measurements respectively.

2.2 Magnetocaloric effect

Magnetic materials placed in a magnetic field, change their magnetization when they are heat up or cold down. This effect is called "magnetocaloric effect".

A magnetocaloric pump using ferrofluids in a micro-fluidic scale was proposed by Love et al. [5] using nanoparticles of (average particle size between 6 and 20nm). They compared thermal and magnetic properties of magnetite suspended in oil-base and water-base, fluids with a Curie temperature in the order of 150°C. Experiments were performed with these two types of ferrofluids, taking the magnetic field, heat input and temperature gradient as constant variables. Love reported a maximum velocity of 2.1 mm/s, for this particular experimental conditions with a temperature gradient of 13°C in the water based-fluid. Table 1 summarizes Love's results [5].

Table 1: Comparison of different ferrofluid in oil and water-based suspension [5]

Material	Specific Gravity	Viscosity (mPa-s)	M_s (Gauss)	T_{low} (°C)	T_{high} (°C)	Fluid Vel. (mm/s)
Magnetite (Fe_3O_4) in oil	1.4	375	350	74	86	0.17
Ferrite ($Mn_{0.5}Zn_{0.5}Fe_2O_4$) in oil	1.52	380	250	48	61	1.59

Ferrite ($Mn_{0.5}Zn_{0.5}Fe_2O_4$) in water	1.37	83	110	46	59	2.1

The results obtained by Love *et al.* [5], verified that the Mn-Zn ferrite is more adequate for magnetocaloric energy conversion than magnetite. As is shown in table 1 velocities are in the order of ten times higher for the Mn-Zn ferrite ferrofluid.

Cataño J.E [7] fabricated a preliminary magnetocaloric pump device running in an open circuit array and showed that it is possible to reach a pressure gradient via the magnetocaloric effect. They synthesized a Mn-Zn water base ferrofluid by using the co-precipitation method, and used the surfactant bi-layer technique in order to reach dispersion of nanoparticles.

The magnetic properties of the ferrofluid at different Mn concentrations and different volumetric concentrations was measured and compared in order to find the maximum ferrofluid magnetization value. Table 2 summarizes their results.

Table 2: Summary of magnetic characterization of different synthesized ferrofluids [8]

Ferrofluid Composition x	ϕ (%)	Density (kg/m³)	M_s (emu/g)	M_s (A/m)	K (A/m°C)	d low fields (nm)	d high fields (nm)
0.5	2.91	1119	2.72	3052	8.95	5.50	4.54
0.7	2.54	1110	4.91	5450	20.1	13.60	5.55
0.8	1.54	1061	3.10	3284	13.1	12.79	4.44
0.5	1.34	1052	0.0945	994	7.15	7.65	4.72
0.7	1.34	1052	2.47	2546	10.2	14.0	6.82
0.8	1.34	1052	2.68	2819	9.05	17.8	8.01

The highest saturation magnetization of the ferrofluid was reached at a Mn concentration of 0.7 using a volumetric concentration of 2.54 %.

Shuchi, *et al.* [11], experimentally determined how the effect of the magnetic field location affects the heat transfer and driving force characteristics of a heat transport device. Such heat transport device uses the pressure gradient due to magnetization losses as the fluid temperature increase. He employed Mn-Zn ferrite nanoparticles dispersed in kerosene and n-hexane with low boiling temperature as the working fluid; the boiling saturation temperature of the fluid was 365K, having a mass concentration of n-hexane of 20%, where the decomposition temperature of the surfactant was calculated as 500K. Three different magnetic field locations were tested and it was determined that the heat transfer and driving force increase when the magnetic field was placed closer to the entrance of the heating section, while at the exit position the result was opposite. In center position, the pressure difference increased only at lower magnetic field intensity. A schematic of the testing section is presented in figure 11.
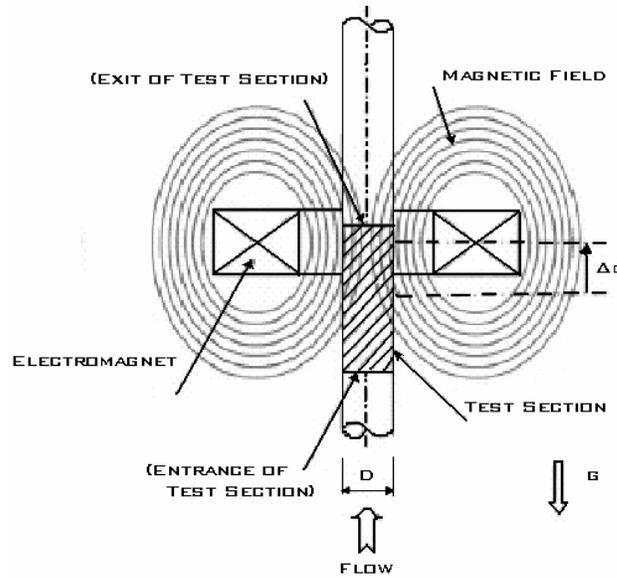
Figure 11: Testing Section Schematic

In this particular experiment the testing section remains constant (unmovable), while the electromagnet is being move at different locations.

Another micropump device able to pump a fluid, but working under a different principle is a magnetohydrodynamic pump.

V. Lemoff [12] developed an AC magnetohydrodynamic (MHD) micropump capable to pump an electrically conducting fluid (NaCl) using Lorentz force. (Force produced when an electric current is applied across a channel filled with conducting solution in the presence of a perpendicular magnetic field). They performed the flow measurements by mixing salt solution with 5μm polystyrene beads and by recording a five seconds movie by employing video capture software. The measures were perform by varying the NaCl concentrations and the pump experiments were carried out varying both, the magnetic

field and the relative phase between the channel current and the magnetic field, where the magnetic field strength of the electromagnet was measured by using a gaussmeter. They demonstrate that is possible to pump a continuous flow with no moving parts. The maximum flow velocity (1.51 mm/s) and the maximum flow rate (18.3 μl/min) were observed for a 1 Mol NaCl solution.

A MHD pump fabricated with low temperature co-fired ceramic tapes (LTCC) was designed by Zhong, Yi, and Bau [13]. They demonstrated that magnetic forces can be used not only for pumping purposes but also to induce the complex flow patterns needed to stir the fluid and enhance mixing [13].

2.3   Synthesis and characterization of ferrofluids

R.D.K Misra, [14] characterized Ni-Zn, Mn-Zn and Mn-Ni ferrites synthesized by the reverse micelle technique (spheroidal micelles formed when a surfactant is dissolved in an organic solvent), they reported that Mn-Zn ferrite ferrofluid presented superior magnetic properties with a saturation magnetization of 9 emu/g when compared with the Ni-Zn and Mn-Ni ferrites (4.5 emu/g and 7emu/g respectively). Mn-Zn showed a singular decomposition to Fe_2O_3 at temperatures above 200°C and reformation at temperatures above 900°C. HRTEM (High Resolution Transmission Electron Microscope) showed particle size in the range of 25-40 nm for all the cases which suggested that the particle size was independent of the ionic solution. All nanocrystaline ferrites revealed the absence of remanence, coercivity, which suggest superparamagnetic behavior.

Arulmuragan *et al*. [6] produced $Mn_{1-X}Zn_XFe_2O_4$ ferrites nanoparticles used for ferrofluid preparation by using a chemical co-precipitation technique. Aqueous solutions of $MnCl_2$, $ZnSO_4$ and $FeCl_3$ where added to the boiling solution of $NaOH$ (0.64 Molar weight) in order to produce the ferrites nanoparticles. Then, after using NH_3 and distilled water to remove impurities, the particles were centrifuged at 5000rpm for 2h and dispersed in heptane using oleic acid as the surfactant, where the volatile nature of the base-fluid helps to increase the particles concentration in the ferrofluid. In order to characterize both, the particles and the fluid, TG-DTA, XRD, TEM, VSM and Mossbauer spectroscopy techniques were employed. The average particle diameter were determined to be 11.3, 10.7, 10.12, 9.2 and 8.5nm for a x=0.1, 0.2, 0.3, 0.4, and 0.5 respectively where agglomeration of the prepared fine particles can beseem for the largest values of zinc concentration (due to the smaller size particles experiences a permanent magnetic moment proportional to their volume). The maximum specific magnetization measured at 10KOe was found to be 48 emu/g for x=0.2 and it decrease when the Zn concentration increase. Figure 12 shows the magnetization in emu/g for different Zn concentrations.
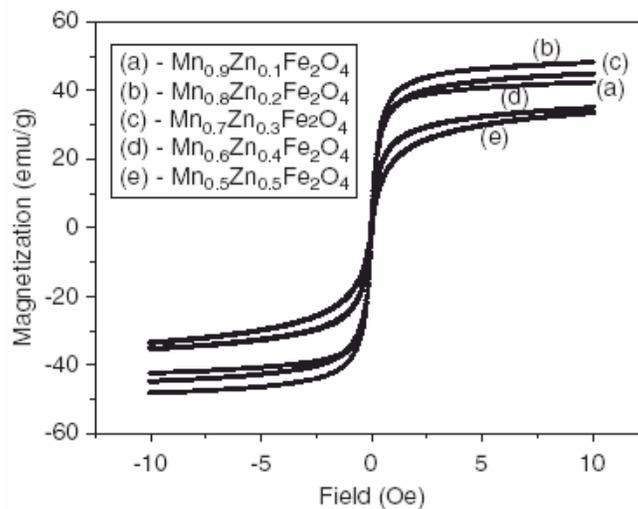

Figure 12: Hysteresis curves of the prepared samples measured at room temperature [10]

25

The magnetic properties of the Mn-Zn ferrites were found to be size dependent and even when the removal of the water content lead to increase the Curie temperature of the precipitated nanoparticles. It was concluded that using $Mn_{0.5}Zn_{0.5}Fe_2O_4$ helps in reducing The Curie temperature can be used for the temperature-sensitive ferrofluid preparation. Table 3 summarizes the magnetization values for different Zn concentrations as well as it correspondent Curie temperature for both the powder and the ferrofluid.

Table 3: Summary of magnetization results

Sample composition	Magnetic parameters measured at room temperature for the powder samples in a field of 10 kOe			Estimated Curie temperature in (°C)	Saturation magnetization of the fluid samples in (Gauss)
	M_S (emu/g)	M_r (emu/g)	H_C (Oe)		
$Mn_{0.875}Zn_{0.099}Fe_{1.94}O_4$	42	2.0	13.0	360	130
$Mn_{0.789}Zn_{0.210}Fe_{1.96}O_4$	48	1.5	9.0	342	148
$Mn_{0.699}Zn_{0.295}Fe_{1.98}O_4$	45	1.3	8.7	303	135
$Mn_{0.591}Zn_{0.399}Fe_{1.96}O_4$	35	0.7	8.6	196	115
$Mn_{0.499}Zn_{0.495}Fe_{1.99}O_4$	34	0.5	8.7	160	120

H. Srikanth [15] compared the magnetic properties of Mn-Zn ferrite using bis-sodium sulfosuccinate (AOT) and a mix of nonylphenol oxyethilene$_5$ and nonylphenol oxyethilene$_9$ (NP) as surfactants. The stoichiometry of sample Mn-Zn ferrite coated with AOT (MZFO-AOT) was established as $Mn_{0.68}Zn_{0.25}Fe_{2.07}O_4$ and $Mn_{0.65}Zn_{0.38}Fe_{1.98}O_4$ for MZFO-NP sample. XRD (X-ray Diffraction) characterization indicated the size for MZFO-AOT being 14.6 nm and 10.8 nm for the MZFO-NP case, and a calculated saturation magnetization at 300K of 57 emu/g and 44 emu/g, respectively. These values increased up to 88 emu/g and 71 emu/g, respectively, at 10K. Such results suggest a

benefit in magnetization when increasing the particle size as consequence of using a coating agent.

The work presented by Vékás [16] explains the procedures for the preparation of concentrated magnetic fluids using water and C_3-C_{10} alcohols (propanol, decanol) as the carrier liquids. Magnetite was produced by precipitation method using NH_4OH as precipitant. No surfactant was used for the water based ferrofluid but a procedure of double layer sterical stabilization (DBS+ DBS; 80°C) + electrostatical stabilized F_3O_4 nanoparticles+ ultrasonic baths was carried out to stabilize the particles and prevent agglomeration. For the C_3-C_{10} alcohol based ferrofluid a saturation magnetization between 800 to 900 Gauss was reported being the highest values obtained, while the water base fluid showed a saturation magnetization near to 400 Gauss but their stability decrease when increasing volume fraction of particles. The water-based ferrofluids were unstable indicating the need of a surfactant. Figure 13 shows the effect of the surfactant in the ferrofluid.
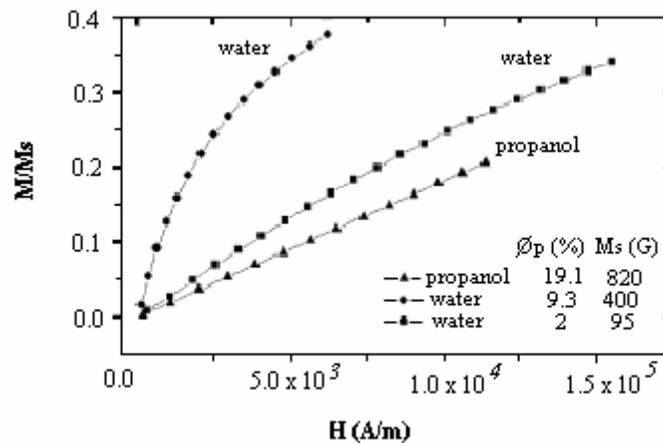

Figure 13: Low Field Reduced Magnetization Curves [9]

It was observed that when the water-based ferrofluid was treated with the surfactant a saturation magnetization of 400 Gauss is obtained, instead the 95 Gauss obtained from the non-surfactant treated water based one.

Auzans *et al*. [4], synthesized and characterized Mn-Zn ferrite ($Mn_{1-X}Zn_XFe_2O_4$) ferrofluid. Aqueous cationic ferrofluids and a surfacted hydrocarbon based ferrofluid were produced via the co-precipitation method of aqueous solutions of $MnCl_2$, $ZnCl_2$ and $FeCl_3$ mixtures in an alkaline medium. Three different alkaline solution were used: Sodium hydroxide (*NaOH*), methylamine (CH_3NH_2) and ammonia (NH_3). It was concluded that increasing the Zn concentration leads to the formation of smaller particles (for the sodium hydroxide and methylamine). The Scherer's formula from X-ray diffraction data was used in order to estimate the particle dimensions. The ferrofluid nanoparticles synthesized with *NaOH* presents the biggest size, while the smallest ones were found when using ammonia. Figure 14 shows the particle size and its correspondent base fluid.
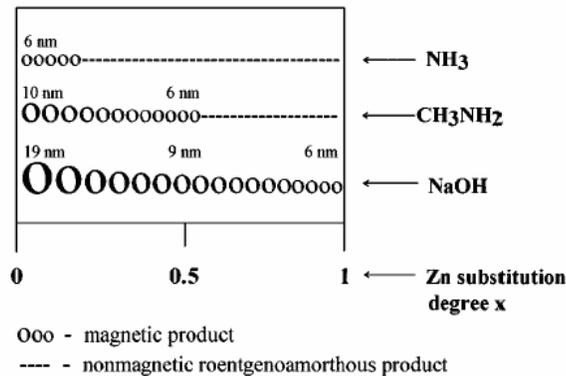

Figure 14: Particle size and base fluid comparison [4]

For CH_3NH_2 and NH_3 formation of ferrite particles is limited to a specific range of Zn substitution: with $0 \leq X \leq 0.5$ and $0 \leq X \leq 0.2$. The maximum value of magnetization obtained was 49 emu/g for X=0.5, where additional increase of Zn showed significant decrease in magnetization.

L.M Pop [17] studied the long time behavior of different magnetic fluid placed in low-gradient magnetic fields using time intervals between 10min and 10h. This study was based on the Gouy Measurement method [17]. The experiment was carried out using stable magnetite ferrofluids coated with oleic acid and dispersed in kerosene.

A decrease of ferrofluid magnetization was observed when increasing magnetic field intensity and exposure time. A low detriment in saturation magnetization of 30%, 20% and 10% respectively was obtained of which 20%, 10% and 8% respectively was attributed to clustering of nanoparticles. The wider the distribution of particle size is the less stable the ferrofluid, in other words, the larger is the distribution of particles size, the higher is the ferrofluid magnetization detriment A quasi-equilibrium of the ferrofluids makeup was obtained after 10 hours [17].

3. METHODOLOGY

3.1 Nanoparticles synthesis and ferrofluid preparation

Prior the ferrofluid preparation, synthesis of suitable nanoparticles was conduced. Iron(III) chloride Hexahydrate (FeCl$_3$.6H$_2$O), Manganese(II) chloride Tetrahydrate (MnCl$_2$.4H$_2$O) and Zinc chloride (MnCl$_2$) were the metallic salts employed in the synthesis process of the $Mn_xZn_{1-x}Fe_2O_4$ particles, while sodium hydroxide (NaOH) at

0.5 mol/L was used as the co-precipitant agent. The metallic salts mixture was added to the pre-heated co-precipitant solution. Keeping constant fluid volume and temperature conditions the reaction time for the ferrite nanoparticles formation was approximately 1 hour under a strong agitation rate. The synthesis process was scalable and the amount of nanoparticles obtained increased from 1.3grams to 10.4 grams. A schematic of the synthesis procedure is shown in figure 15.
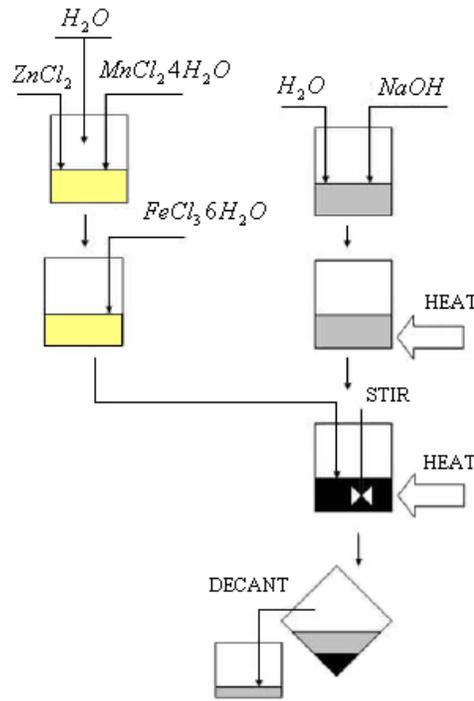
Figure 15: Synthesis Procedure Diagram [9]

The nanoparticles obtained were washed with a 2mol/L nitric acid (HNO_3) solution and centrifuged after manual agitation at 3600rpm for a seven minutes period, where the nitric acid cleans and provides the nanoparticles surface with a positive electrostatic charge (first layer). Then a 25 % water solution of tetramethylammonium hydroxide is slowly added to the cleaned particles providing them of a negative surface electrostatic charge (second layer) and thus completing the double-layer surfactant effect and inhibiting their agglomeration and further sedimentation. The mixture of the water,

surfactant and nanoparticles is again strongly agitated prior a twelve minutes centrifugation process at 3600rpm.

A Siemens D500 diffractometer was used to verify the ferrite structure formation (X-ray diffraction is a technique which reveal information about the crystallographic structure, chemical composition, and physical properties of materials and thin films based on observing the scattered intensity of an x-ray beam hitting a sample as a function of incident and scattered angle, polarization, and wavelength). While nanoparticles and ferrofluid magnetic properties were obtained by using a Super Quantum Interference Device (MPMS XL-7 SQUID magnetometer with an AC susceptometer consisting of two superconductors separated by thin insulating layers to form two parallel Josephson junctions and configured as a magnetometer able to detect incredibly small magnetic fields). Such results are presented in chapter 4.

The following is a detailed systematic procedure for the ferrite synthesis process. Table 4 shows the materials required to produce Mn-Zn ferrites with a Zinc substitution of x=0.3

Table 4: Material list for synthesis of ferrite nanoparticles

Item	Qty	Description
Beakers	2	2000ml Stainless Steel
Burners	1	Propane burner
Stirrer	1	400 series Fisher Sci.
Stirrer Paddle	1	Fisher Scientific (PVC)
Thermometers	1	Fisher Scientific (Mercury)
Thermometers Clamps	1	Fisher Scientific
Agitation Paddle	1	6" long Fisher Sci.
Digital Balance	1	Fisher Scientific

Glass Cylinder	1	Numbered 250ml
Beaker holder	1	Costume made
Sodium Hydroxide	15.64g	Sigma-Aldrich
Manganese (II) Chloride Tetrahydrate	13.2967g	Sigma-Aldrich
Zinc Chloride	0.9728g	Sigma-Aldrich
Iron(III) chloride Hexahydrate	12.6g	Sigma-Aldrich
Distilled Water	1224ml	N/A
Weighing Paper	5 sheets	N/A
Cleaning wipes	5 sheets	Kimwipes
Globes	1pair	High Resistant Latex

A 2000mml beaker is filled with 800ml of distilled water and the 15.64g of NaOH are added inside it. Another 2000ml beaker is filled with the $FeCl_3.6H_2O$, $MnCl_2.4H_2O$ and $MnCl_2$ composites within 256ml distilled water while the NaOH solution is being preheated by using the burner under an agitation rate of 150rpm. The thermometer is clamped to the beaker and the stirrer paddle is used as a level indicator. Once the NaOH solution reaches 100ºC, the salts solution is slowly added. The agitation rate is increased to approximately 900rpm and the reaction time begins when the solution reaches the boiling point. The volume of the solution must be maintained constant by adding small amounts of distilled water periodically. One hour later, the beaker is removed and the ferrites are ready to be suspended. Table 5 shows the equipment required for ferrofluid preparation.

Table 5: Ferrofluid preparation material's list

| Item	Qty	Description
Benchtop Centrifuge	1	Thermo IEC* Centra* CL2
Ultrasonic cleaner	1	Fisher Sci. FS6
Precision Probe	1	Playtex 25ml
HNO_3	100ml	2 mol/L solution
Tetramethylammonium hydroxide	40ml	Alpha Aesar-25% water solution

For ferrofluid preparation, the nanoparticles are removed from the water used for the synthesis process and deposited in the 50ml Benchtop Centrifuge recipients. Now the recipients containing the nanoparticles are filled with the HNO_3 solution and cleaned by 15 minutes in an ultrasonic bath. Then, the washed ferrites are centrifuged as described before. The process is repeated three consecutive times until the ferrites have been completely cleaned and positively charged. Thus, Tetramethylammonium hydroxide is slowly added by using the 25ml precision probe. The resultant colloid is the ferrofluid and the sediment is discarded. Usually the nanoparticles suspension process takes approximately two hours to obtain 32ml of ferrofluid.

The total time needed to produce the ferrofluid change from seven hours to three hours and the amount of ferrofluid increased from 4ml to 32ml by scaling the process

3.2 Magnetocaloric pump design

Several MCP prototypes were designed in order to demonstrate the magnetocaloric effect principle. All of them used a 45W heater as the external heating supply and different sizes (½ inches, 1inch and 2 inches diameter.) 0.35-0.5Tesla magnets as the external permanent magnetic induction source (the permanent magnetization amounts were measured by using a DC Magnetometer and a AlphaLab Inc. 1-8014879472 Gaussmeter). Each permanent magnet has a cylindrical shape with a 5/16" center hole where a cooper tube is passed through.

One of the first designs was composed of a cooling system as shown in figure 16. Thermocouples type K were inserted into 2 cooper barber crosses. The main section was fixed by using pressure cooper nuts, Teflon bands and various quick connect line-to-line fittings. A cast iron globe valve and a standard cooper tee were implemented for the purge process.
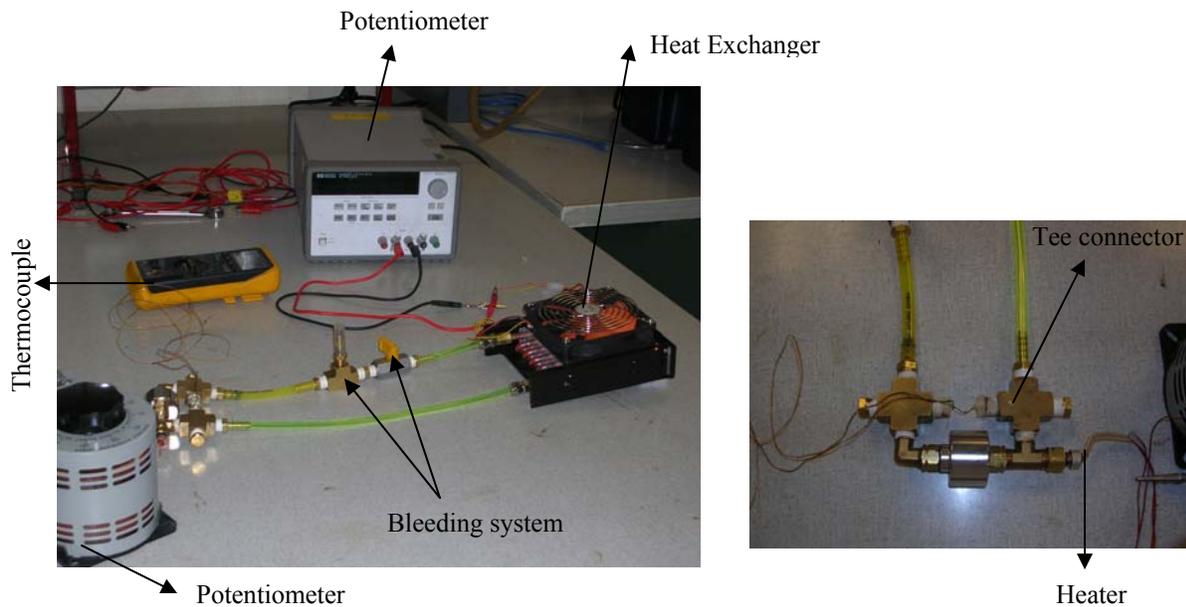
Figure 16: Preliminary Magnetocaloric Pump design 1.1

Trying to reduce friction losses some connections were removed. The tubing length was considerably reduced and eventually the cooper connections were replaced for push-in PVC connections. In addition, a new cooling system was manufactured in order to increase the heat transfer process. Figure 17 and figure 18 show two of those preliminary designs. Some of the addition materials includes Plexiglas, small auto tighten traps, high temperature resistant epoxy and silicon
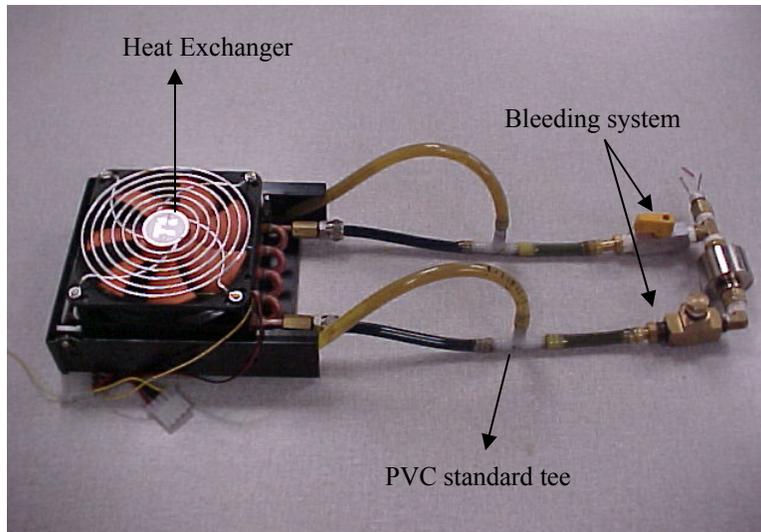
**Figure 17: Preliminary Magnetocaloric Pump design 1.2**
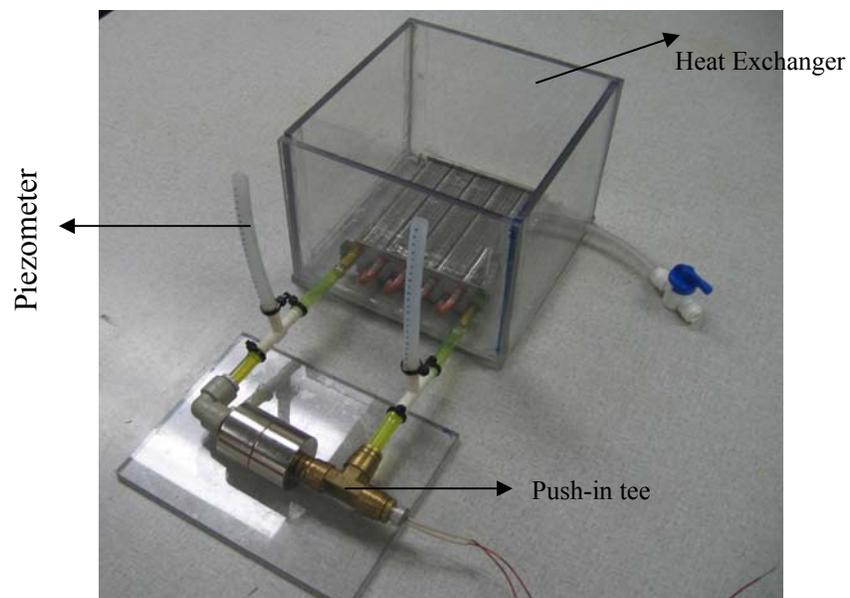
Figure 18: Preliminary Magnetocaloric Pump design 1.3

Finally, the prototype selected to demonstrate the magnetocaloric effect is shown in the

figure 19.
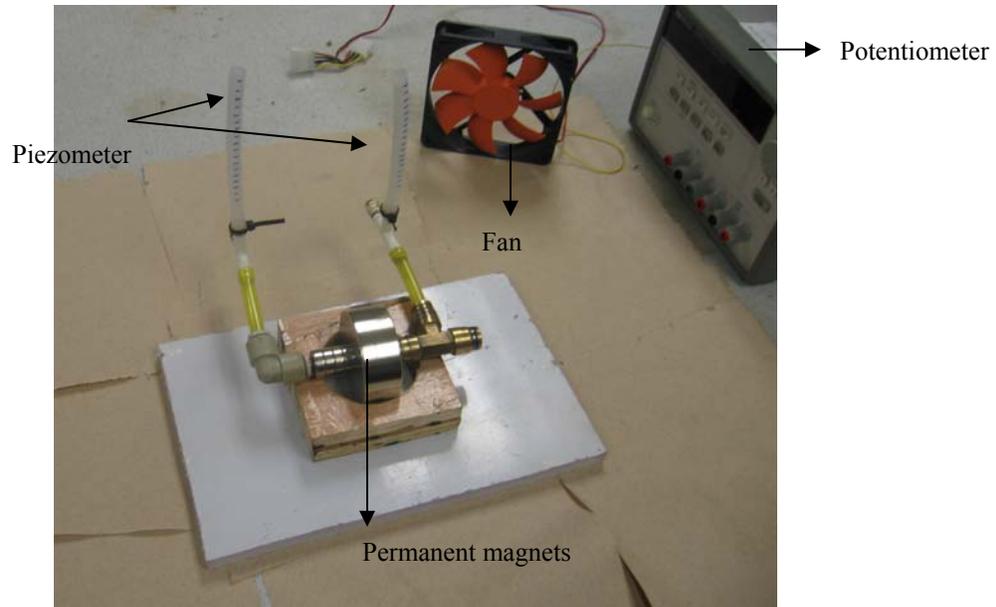
Figure 19: Final Magnetocaloric Pump Design 1.4

Due to the system implemented to measure the pressure head, the system was decided to operate in an open loop. A 120mm X 120mm, 12Vcommercial fan was employed for the cooling down process. The system is mounted over two dissimilar insulated materials to avoid magnetization losses through other devices. In the final design, the 1/8", 45 W heater is placed inside the cooper tube (10cm long) and connected to a 120V variable potentiometer. Two Polyvinyl chloride (PVC) Parker push-to-connect elbows connect the central section with the tubing lines where two plastic tees and two piezometers are employed in order to measures the pressure gradient generated by the pump. High resistant ¼ ID tubing completes the system.

Bleeding process is often required and a 12V fan connected to a digital 30V power supply is used to accelerate the cold down process. Figure 20 shows the magnetocaloric

pump prototype schematic (see Appendix B for detailed description of final design) and

table 6 summarizes the mayor advantages and disadvantages of each preliminary

prototype

Figure 20: Magnetocaloric pump prototype

Table 6: MCP design process summary

Prototype	Advantages	Disadvantages
1.1	▪ Thermocouples inside tubing ▪ Heat exchanger	▪ Long tubing system ▪ Ineffective bleeding method ▪ 3-recirculation zones ▪ Too many fittings
1.2	▪ Heat exchanger ▪ Pressure measurement system	▪ Ineffective bleeding method ▪ Too many fittings ▪ Flexible tubing promotes change in Δz ▪ Long tubing system
1.3	▪ Push-in fittings ▪ Rigid tubing system ▪ Heat exchanger	▪ Long tubing system ▪ Heater inside tubing
1.4	▪ Push-in fittings ▪ Rigid tubing system ▪ Very short tubing system ▪ Effective bleeding process	▪ Heat exchanger ▪ Open loop system ▪ Heater inside tubing system

4. RESULTS AND ANALYSIS

4.1 Nanoparticles characterization

Synthesis of $Mn_xZn_{1-x}Fe_2O_4$ was carried out using the co-precipitation method. X-ray diffraction (XRD) was employed to verify the formation of Mn-Zn ferrites crystalline structure. Each particular solid has its unique characteristic x-ray pattern that allows its identification. The Mn-Zn ferrites were obtained using a conventional hot plate (400°C) in a 5 hours reaction process and a constant agitation rate of 500rpm. The produced nanoparticles were compared with ferrites synthesized using a burner after 1-hour reaction time and a constant agitation rate of approximately 900rpm. The XRD data for the solids, produced by the two synthesis options as well as for the commercial ferrofluid are presented in figure 21.
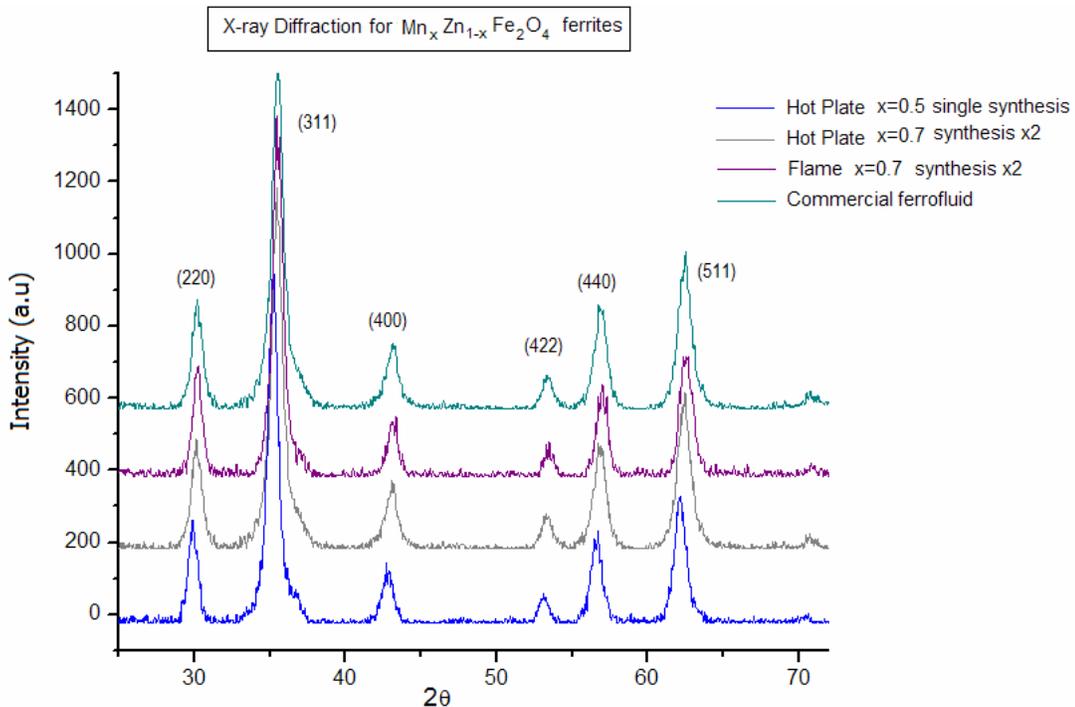

Figure 21: XRD measurement for Mn-Zn ferrites

All peaks correspond to a ferrite structure. The evidence of ferrite formation is corroborated when the (220), (311), (400), (422), (440) and (511) peaks appears in all the cases [6, 21]. Such information suggested the processes could be scalable at least in terms of ferrites structure formation. In addition, it is observed a small delay in the ferrites produced at x= 0.5 when compared with the x=0.7 ones due to the zinc substitution in accordance with Arulmurugan [21]. The Scherer's formula was employed to estimate the average particle diameter for different Mn substitution values as follows:

$$D_{ave} = \frac{k\lambda}{\beta \cos(\theta)} \qquad (4.1)$$

Where K is the Scherer's constant (0.92), λ is the wavelength of the radiation and β represents the integral breadth of a reflection. Figure 22 shows an schematic of the values obtained after X-ray diffraction.
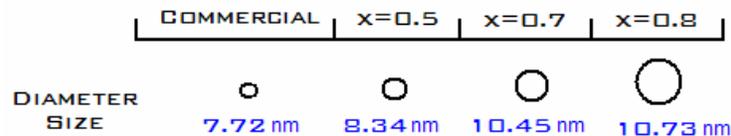
Figure 22: Average crystal size at different values of Mn substitution

As expected, the higher the atomic ratio "x" (bigger Mn amount), the larger the average crystalline size. This result is in good agreement to Auzans [23] and Calderon [9] works.

In order to complement the XRD results, the Mn-Zn ferrite structure formation (using a burner as the heat supply system) was investigated by Fast Transform Infrared

spectroscopy (FTIR)[*]. FTIR spectroscopy is a measurement technique whereby spectra are collected using time-domain measurements of the electromagnetic radiation. The wavelength of light absorbed is characteristic of the chemical bond. Molecular bonds vibrate at various frequencies depending on the elements and the type of bonds and by interpreting the infrared absorption spectrum, the chemical bonds in a molecule can be determined. FTIR spectra of pure compounds are generally so unique that they are like a molecular "fingerprint". Figure 23 and 24 show the results obtained after 30min and 1-hour synthesis period, respectively.
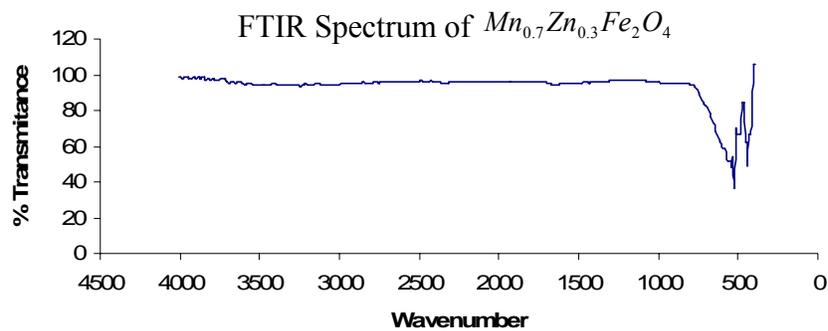

**Figure 23: Ferrite structure formation after 30min**
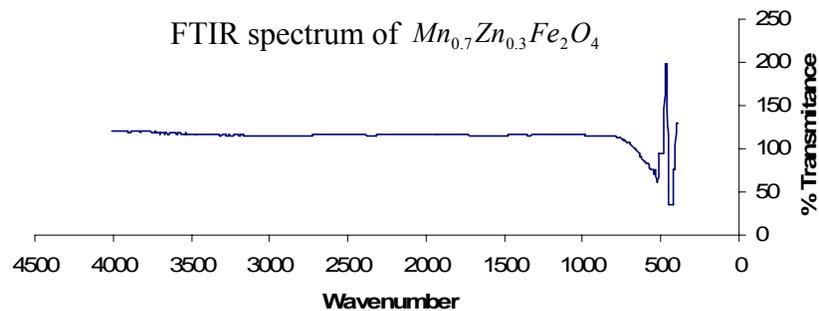
Figure 24: Ferrite structure formation after 1hour

Although both behaviors (characteristic bands coincident at 540 cm^{-1}) suggest the ferrite

structure formation [23], after one hour of reaction time the ferrites nanoparticles appear

to be almost free of intermediate compounds. Therefore, the synthesis process to obtain

the nanoparticles was settled at 1-hour for mass production purposes.

The magnetic properties of the powder were measured using a Super Quantum

Interference Devise (MPMS XL-7 SQUID magnetometer with an AC susceptometer).

The saturation magnetization of the produced ferrites as well as the change in

magnetization with respect to the temperature obtained for both the commercial and the

$Mn_xZn_{1-x}Fe_2O_4$ produced nanoparticles are presented in figures 25 and 26 respectively.

Figure 25 shows the M-H curve for a Mn substitution of 0.7.

In strong agreement with literature [4, 5, 6] the saturation magnetization of the powder

nanoparticles for a Zn substitution of 0.3 resulted to be 42.66 emu/g (46074.41 A/m). The

experiment was conducted at a temperature of 325K (estimated operational temperature

of the pump) for a maximum induced field of 20,000Oe until saturation
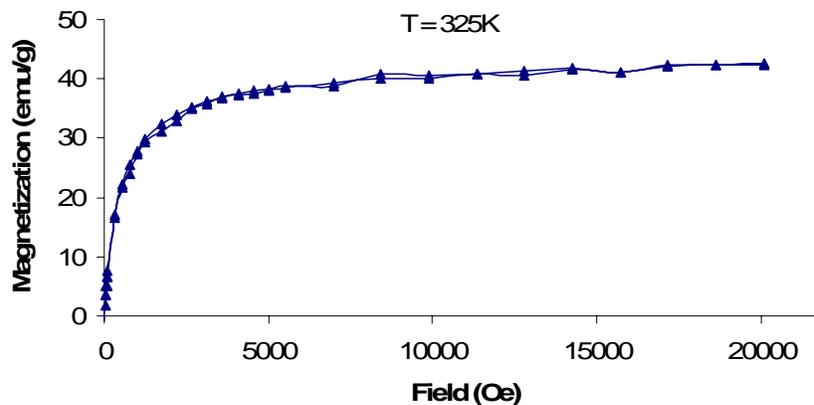
Figure 25: M-H curve for produced nanoparticles x=0.7, ϕ =1.52%
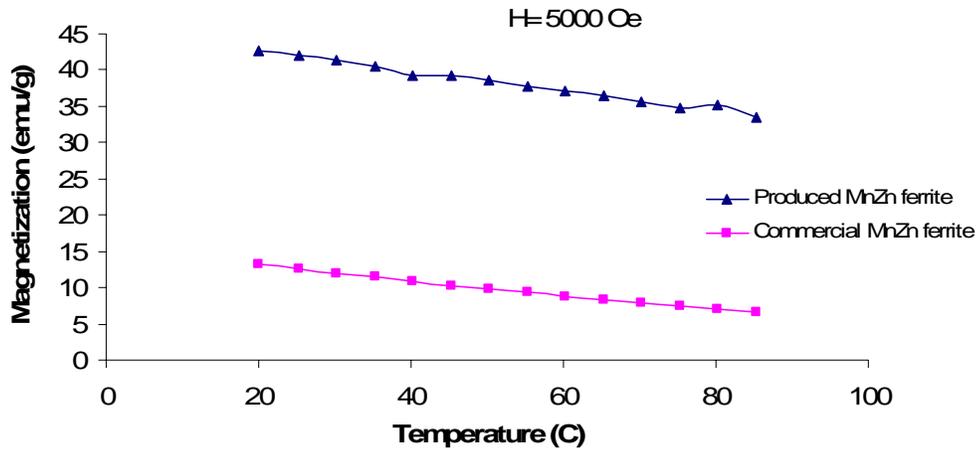
Figure 26: M-T curves for produced and commercial nanoparticles

Figure 26 shows the magnetization vs. temperature for both, the produced MnZn ferrite nanoparticles and the commercial MnZn ferrite nanoparticles. As expected, temperature effect misaligns the dipolar magnetic moments of the particles with respect to the applied magnetic field, resulting in a reduction in the particles net magnetization for both produced and commercial Mn-Zn nanoparticles. Both tests were carried out at 5000Oe external field, which is the operational applied magnetic field used in the MCP prototype and the temperature was increased in intervals of 5ºC from 20ºC to 90ºC. The commercial ferrite nanoparticles were obtained after drying the ferrofluid for 4 hours at 80ºC. Usually nanoparticles suspended in organic solvents (hydrocarbons and alcohols) uses acetone as a cleaning agent and oleic acid as the surfactant; then it is possible some of these substances were still present in the magnetization tests, making it seemed considerably lower than the produced ones. This fact could be clarified with the ferrofluid characterization.

4.2 Magnetic Characterization of Mn-Zn ferrofluids

Figure 27 shows the magnetic behavior of both magnetic fluids. The experiments were tested at the same temperature and field than nanoparticles. The produced $Mn_{0.7}Zn_{0.3}Fe_2O_4$ ferrofluid reported a saturation magnetization value of 6182 A/m (5.72emu/g) while the maximum magnetization for the commercial ferrofluid occurred at 9156 A/m (8.03emu/g). Non-saturation condition was achieved for the commercial ferrofluid although the value reported by the manufacturer is 150 Gauss (12188 A/m *or* 11emu/g).
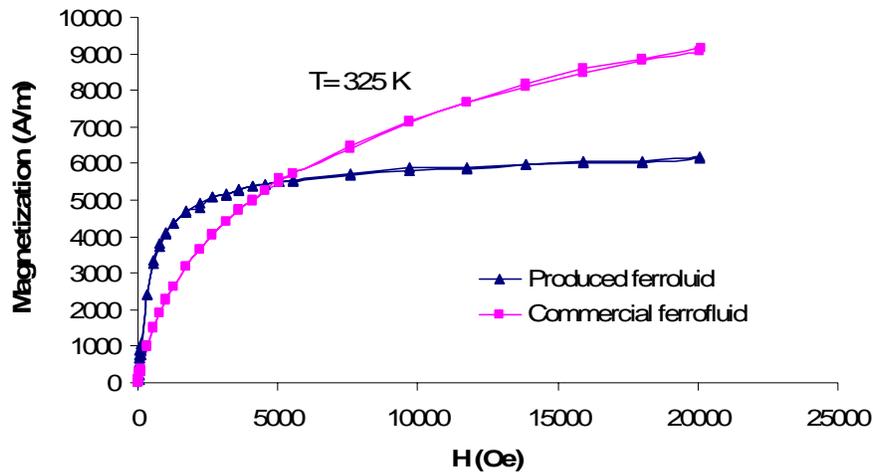
Figure 27: M-H curves for produced and commercial ferrofluids

When a magnetic particle has a very small diameter, its alignment in the direction of the applied magnetic field tends to be difficult. In such cases, the polydisperse condition of magnetic fluids makes possible the alignment of the majority of the nanoparticles but those small ones could cause a non-saturation condition even in the presence of high magnetic fields. This fact could be notice by comparing the initial susceptibility of both ferrofluids; bigger particles are aligned more quickly than the small ones and the slope of

the M-H curve is higher at the beginning. In this case, nanoparticles contained in the commercial ferrofluid seem to be smaller than the produced ones. For this particular case, M_s represents the maximum value obtained from magnetic measurements but not the saturation magnetization of ferrofluid which is reported to be 12.000A/m (11emu/g). Then, for practical purposes, it could be assumed the graph will maintain its ascending behavior until reach the reported value. Section 4.2.1 presents the mean nanoparticles sizes obtained from magnetic measurements and compare it with the X-ray diffraction results.

Similar to the nanoparticles, the ferrofluid magnetization amount shows a decreasing behavior when the temperature increases. Due to the nature of the base fluid the produced magnetic fluid test was conduced until 85ºC (maximum operational temperature of the pump) while the commercial ferrofluid finished ten degrees earlier. Both tests were again carried out in a 5000Oe external field (MCP magnetic induction). Figure 28 shows the temperature effect in the magnetization measurements.
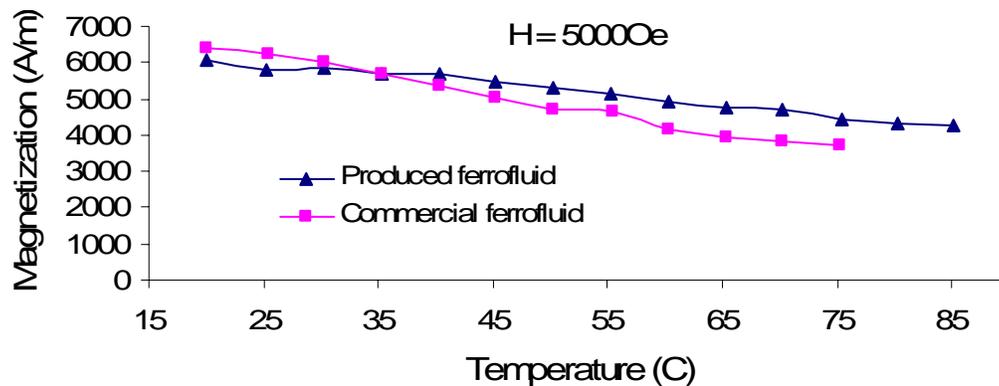

Figure 28: M-T curves for produced and commercial ferrofluids

44

In this particular case, the pyromagnetic coefficient $\left(K = \dfrac{\Delta M}{\Delta T} \right)$ can be thought as the

ability of a ferrofluid to loose it magnetization due to temperature effect. In fact, the

larger the pyromagnetic coefficient, the larger the magnetocaloric effect and the larger

the pressure gradient also. The commercial ferrofluid exhibited a pyromagnetic

coefficient of 48.2 A/mK against the 28.13 A/mK the produced ferrofluid has. According

to these results, and by using the simplified Bernoulli equation for magnetic fluids

(equation 1.19), the maximum possible pressure head when using the produced ferrofluid

should be 7.21cm for a maximum ΔM of 1492A/m (1.42emu/g) available. In the other

hand, the maximum possible pressure head available must be 11.66 cm for a maximum

ΔM 2402A/m (2.40emu/g) by using the commercial ferrofluid. It means that from the

total ideal ΔM given by the fluid just a 24.8% of the produced ferrofluid and a 21.8% of

the commercial Mn-Zn ferrofluid can be used for magnetocaloric energy conversion.

Experimental and theoretical results will be compared and discussed in section 4.3

Another important conclusion obtained from the M-T curves is related to the Curie

temperature. The value of the Curie temperature was estimated by extrapolating the data

from figure 26 for the powder and figure 28 for the ferrofluid until find the interception

with the "x axis" as explained in section 1.3. A lower value of Curie temperature in the

ferrofluid is obtained and it is compared with the powder results performed at the same

experimental conditions. Since the particles are suspended in an aqueous medium it is

easier to misalign them with respect to the applied magnetic field and then a reduction in

the net magnetization is expected when applying a temperature gradient in the ferrofluid.

Brownian motion [1] and van der Waals attractive forces [1] as well as the presence of

other components surrounding the particles (surfactants and cleaning agents) must also be considered in the analysis. Table 7 summarizes the results obtained from the powder and ferrofluid Curie temperature. It can be seen that the Curie temperature in the produced ferrofluid is reduced by 28% when compare it with the powder. However, these results depend on magnetization, nature of solvent, volumetric concentration, particle size and composition; thus, the comparison of the Curie Temperatures could be inaccurate.

Table 7: Curie temperature for powder and ferrofluids

Curie Temperature (ºC)	Produced Nanoparticles	Produced Ferrofluid	Commercial Nanoparticles	Commercial Ferrofluid
	306.5	223	145	126

These results suggest that the Curie temperature is not an intrinsic property of the material. However, it was assume the values obtained from figures 25 and 27 belong to the linear portion of the M-T curve (as presented in figure 6) and it is recommended to run the experiments within a wider temperature range in order to achieve more accurate results.

4.2.1 Estimation of particle size and volume fraction from magnetic measurements

Assuming monodispersity conditions, the particle diameter can be calculated by using the asymptotic values of the Langevin function as follows:

$$\frac{M}{\phi M_d} = \coth \alpha - \frac{1}{\alpha} = L(\alpha) \qquad (4.2)$$

Where
$$\alpha = \frac{mH}{k_B T} = \frac{\pi \mu_0 M_d H d^3}{k_B T}$$
(4.3)

M_d is the domain magnetization (bulk), m is the nanoparticles magnetic moment, μ_0 is the permeability of the free space ($4\pi x10^{-7} H/m$), T is the absolute temperature, k_B is the Boltzmann constant ($1.38x10^{-23} Nm/K$), H is the external magnetic field, and ϕ is the volume fraction.

The initial Susceptibility is given by $\chi_0 = \left.\frac{dM}{dH}\right|_{H\to 0}$ and for low field the particle diameter can be estimated:

$$\chi_0 = \frac{\pi \phi \mu_0 M_d^2 d^3}{18 k_B T}$$
(4.4)

While for high field values, the particle size is obtained from:

$$\frac{M}{\phi M_d} = 1 - \frac{6 k_B T}{\mu_0 M_d H d^3}$$
(4.5)

At low fields, the magnetization is mainly determined by large particles while at high fields the main contribution is performed by the smallest ones. Therefore, the particle diameter tends to be higher when calculated at low fields rather than at high magnetic fields. However, the magnetic properties of a ferrofluid are modified by the fact of particle size distribution; then, the magnetization is given by the sum of the contributions for each particular diameter [22] as follows:

$$M = M_s \int_0^\infty L(\alpha) f(y) dy$$
(4.6)

Where $f(y)dy$ is the fraction of the total magnetic volume having a diameter between y and $y+dy$. Substituting (4.5) in to (4.6) and recalling that for large H values the relation between M and $1/H$ should be a straight line crossing $M=0$ axis at a point $1/H_0$.

$$1 = \frac{6k_BT}{M_d\pi d^3 H_0}\int_0^\infty y^{-3}f(y)dy \qquad (4.7)$$

Thus, after applying a log normal distribution function the particle diameter for a ferrofluid having polydispersed nanoparticles according Chantrell [22]. will be:

$$d = \left[\frac{18k_BT}{\pi\mu_0 M_d}\sqrt{\frac{\chi_0}{3\phi M_d H_0}}\right]^{\frac{1}{3}}$$

(4.8)

Where χ_0, $1/H_0$, ϕ are determined experimentally and M_d is taken as 91 emu/g and 85emu/g for the commercial and produced ferrofluid respectively [25].

Figures 29 and 30 show the commercial ferrofluid M vs. H and M vs. $1/H$ curves for both, low and high fields.
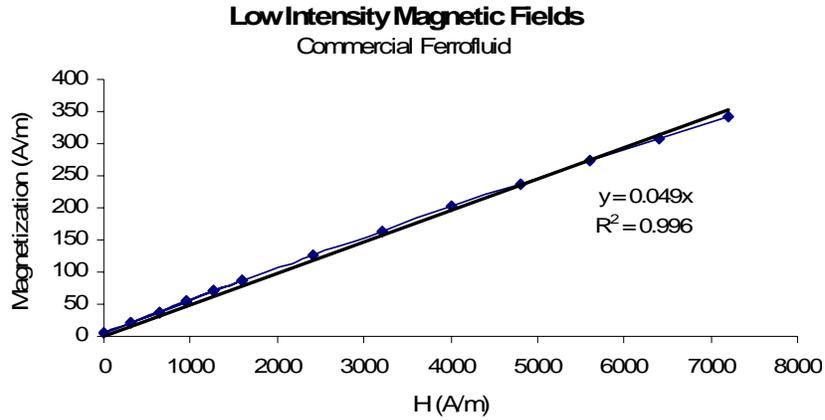
Figure 29: Magnetization curve at low field (H) for commercial ferrofluid
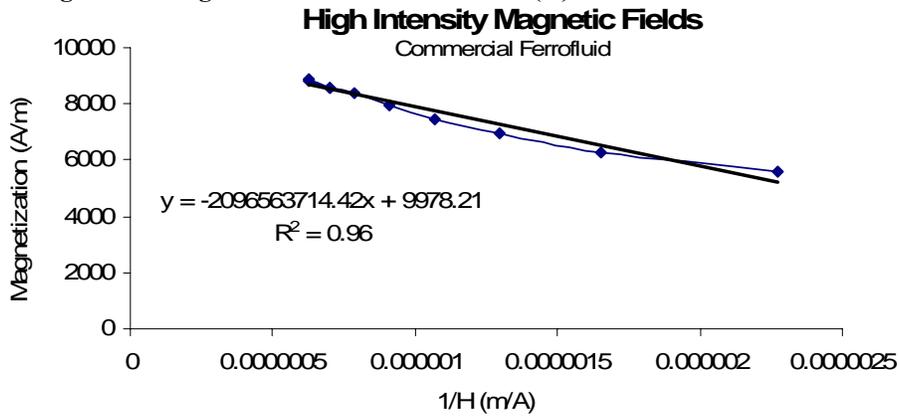
Figure 30: Magnetization curve at high field (H) for commercial ferrofluid

From slope of the curve at low fields the initial susceptibility value (χ_0) is obtained, while H_0 is obtained from the high field magnetic curve slope and the saturation magnetization value. Table 8 summarizes the ferrofluids properties obtained from both, magnetic measurements and X-ray analysis discussed in section 4.1.

Table 8: Ferrofluid Properties

Ferrofluid	$D_{X\text{-ray}}$ (nm)	D_{SQUID} (nm)	Vol. Fraction (%)	Density (kg/m^3)	M_S (A/m)
$Mn_{0.7}Zn_{0.3}Fe_2O_4$	10.45	7.81	1.52	1080	6182
Commercial Mn-Zn	7.72	5.07	2.04	1108	8899

A small difference in the average particle diameter between the XRD and SQUID analysis it is commonly presented due to the XRD results are based on a volumetric analysis while the SQUID tend to underestimate that value assuming the entire particle responds to the applied magnetic field without having on count the particles coating. It is also important to notice that the volatile nature of the commercial hydrocarbon-based Mn-Zn ferrofluid promotes a volume fraction increment and consequently a higher saturation magnetization without sedimentation constraints.

4.3 Magnetocaloric pump characterization

Different important parameters of a device employed for magnetocaloric energy conversion are not taking into account the simplified Bernoulli equation for magnetic fluids. Some of those parameters include the effect of the heat source location, magnetic induction effective area, hydraulic losses, and ferrofluid type effect. Thus, the designed magnetocaloric pump was characterized by testing it effect in the MCP performance.

Figure 31 shows the MCP prototype as explained in section 3.2, working in an open circuit. The heater is located at the left side, inside a copper tee. A 0.5T, 2" diameter

permanent magnet is joined to another four 0.35T, 1/2"diameter permanent magnets

attached to the cooper tube. The two piezometers have 20 divisions of 0.5cm each.
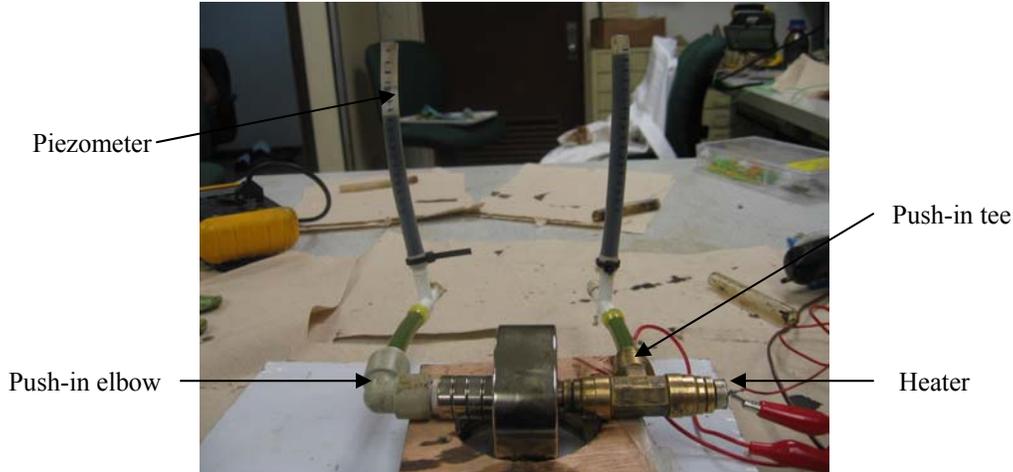
Figure 31: Magnetocaloric pump working with the Mn-Zn produced ferrofluid

Figure 32 and figure 33 shows the variation of heat source location for the hydrocarbon-based and produced water-base ferrofluids respectively obtained experimentally. The initial position corresponds to the rigth side edge of the permanent magnet section; the middle section is located just in middle of the magnets and the ending position at the left side edge, near the push-in PVC elbow connection (see appendix C).
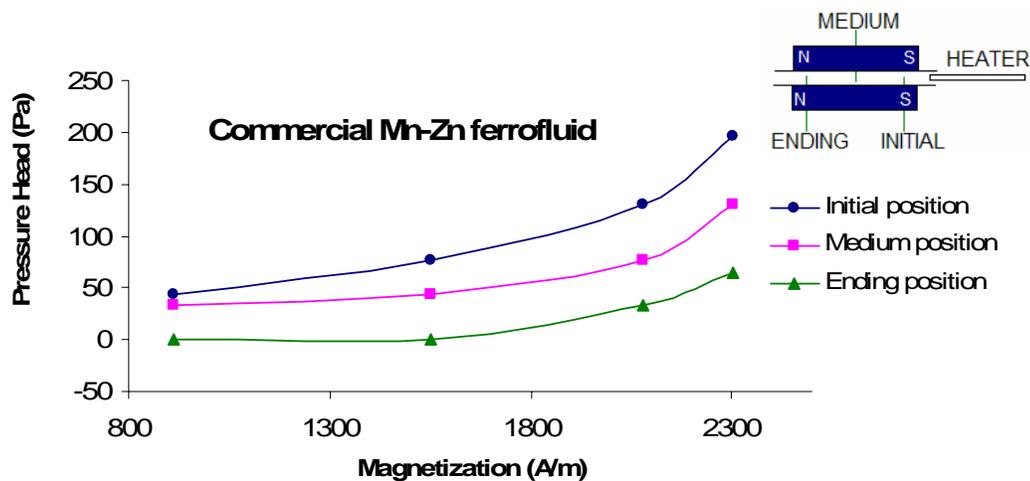
Figure 32: Effect of heat source location for commercial Mn-Zn ferrofluid
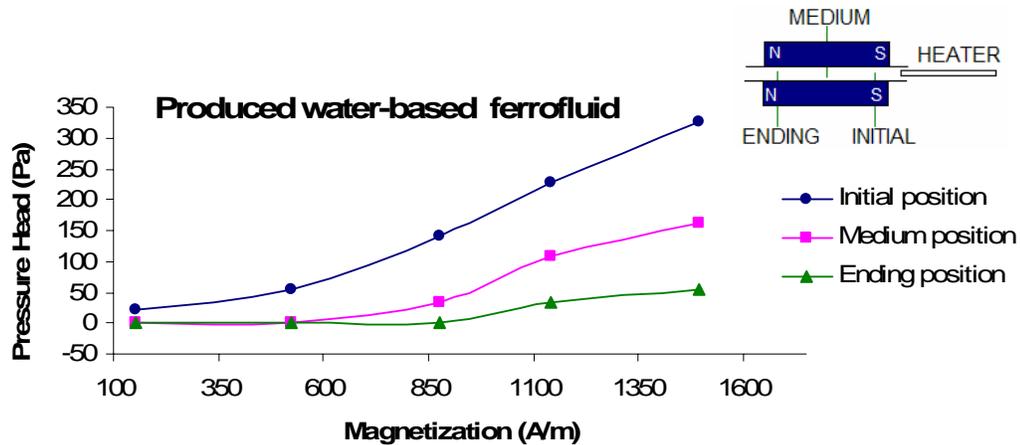
Figure 33: Effect of heat source location for produced Mn-Zn ferrofluid

In agreement with the work performed by Shuchi, *et al* (2004) the magnetocaloric effect quantified by the obtained pressure head was found to be stronger when the heating source is placed at the initial position. The amount of heat induced at different points of the pump propagates by conduction and thermal diffusion to it surrounding rather than be concentrated in a specific point. Then, it is easier for the cold fluid just to push a small quantity of hot fluid instead of big amounts when considering the propulsion system of the pump is not an impeller but the fluid itself. Therefore, the obtained pressure head resulted to be minimum at the ending position due to the portion of magnetic fluid attracted by the magnetic source is poor. In other words, the more the hot fluid inside the magnetic induction area, the less the obtained pressure gradient.

Another important result is related to the maximum pressure gradient reached by the pump when running using both magnetic fluids. Even when magnetic results suggest the commercial ferrofluids to be more convenient for magnetocaloric energy conversion

(highest saturation magnetization and the lower Curie temperature[†]), maximum pressure reached with the water-based ferrofluid resulted to be higher. The effect of the ferrofluid viscosity was found to have significant influence in the system in accordance with the work presented by Love *et al.* (2004). The nature of the base fluid as well as the volumetric concentration for the commercial ferrofluid supposes a higher viscosity value when compared with water-based one. This is found to have remarkable effects in the magnetocaloric effect output and suggest that the simplified Bernoulli equation can involve limitations when the inviscid fluid condition is assumed. Figure 34 show detailed information about the ideal (inviscid) and actual (viscous) pressure gradients obtained after using the commercial magnetic fluid inside the MCP where the effect of viscosity can be noticed.
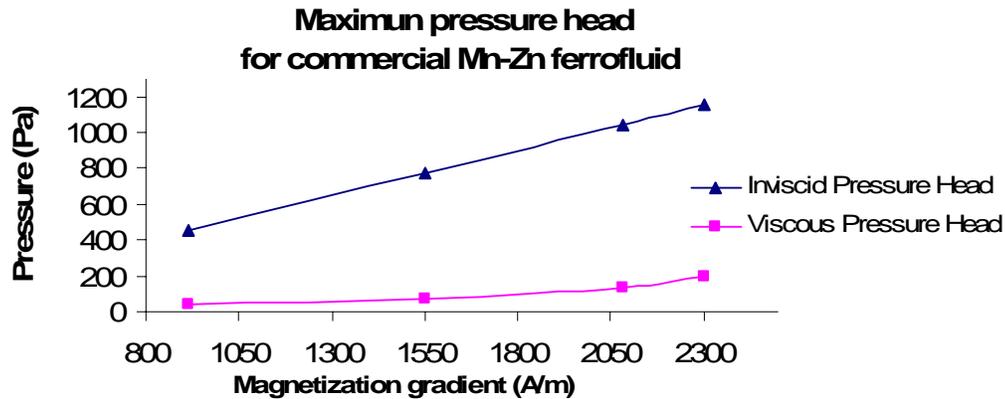

Figure 34: Maximum ideal and actual pressure head for commercial ferrofluid

The maximum pressure gradient in Pa calculated for the commercial ferrofluid according the M-T curve (figure 27) for different ΔM is approximately 1152 while in practice the maximum value was 195.71Pa. This represents only a 17% of the total magnetocaloric energy conversion available for the commercial ferrofluid. Figure 35 shows a similar

---

[†] Base on the M-T curve results for both ferrofluids (figure 27)

behavior when the pump is running with the produced ferrofluid and the effect of viscosity is neglected.
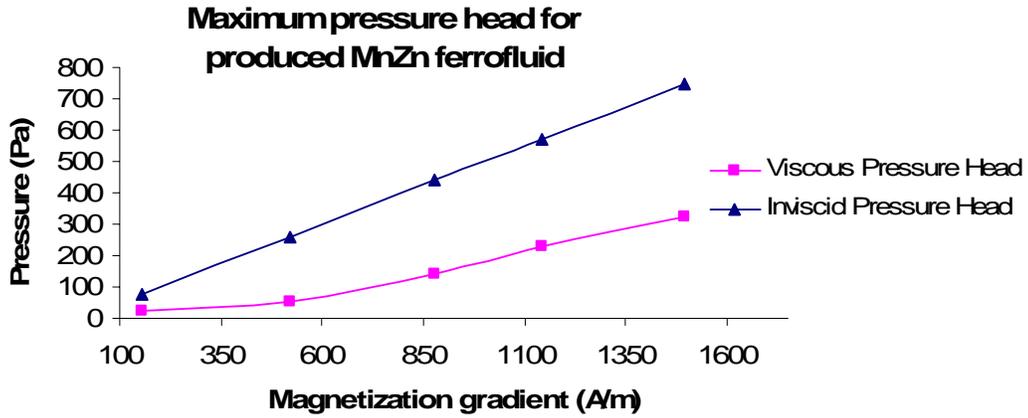
Figure 35: Maximum ideal and actual pressure head for produced ferrofluid

The maximum pressure gradient calculated according the M-T curve (figure 28) for the produced ferrofluid at different ΔM is approximately 746Pa while in practice the maximum value obtained was 326Pa. This represents a 43.7% of the total magnetocaloric energy conversion available when using the produced ferrofluid. Again, it is found strong evidence of the adverse effect of the fluid viscosity in the system performance. Figure 36 shows the pressure gradient comparison between both ferrofluids and table 8 summarizes the magnetic properties and maximum pressure gradient raised for the MCP for different ferrofluids.
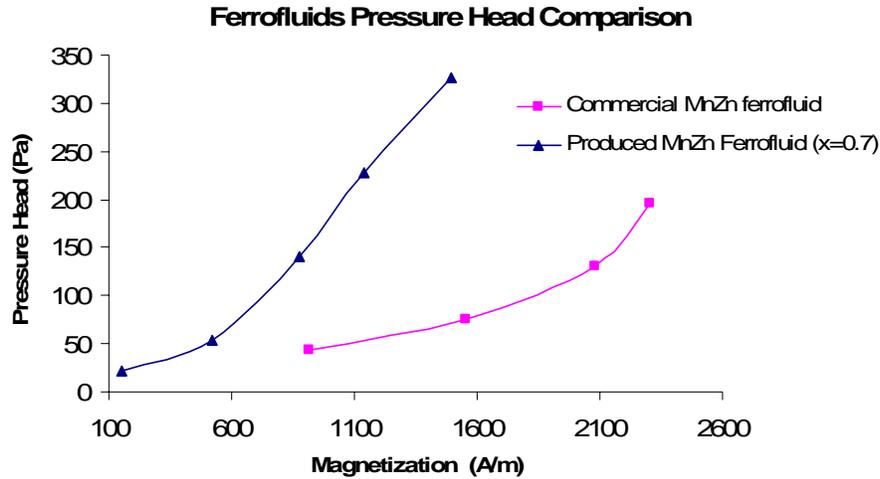
Figure 36: Ferrofluids pressure head comparison

The volatile nature of the commercial base fluid (hydrocarbon-based) not only propitiates the increase in the volume fraction and the viscosity of the ferrofluid, but also limits the operational temperature range and hence, the MCP applicability. Thus, ferrofluids synthesized by using organic solvents as the base fluid have been shown to be poor for magnetocaloric applications near to the ambient temperature even when having higher magnetization and pyromagnetic coefficient than the water-based ferrofluids.

Table 9: Physical properties and maximum pressure gradient for different ferrofluids

Ferrofluid	ϕ (%)	ρ (kg/m^3)	M$_s$ (A/m)	ΔP (Pa)
Commercial ferrite in hydrocarbon	2.04	1108	12,000	195.71
Ferrite ($Mn_{0.7}Zn_{0.3}Fe_2O_4$) in water	1.52	1080	6182	326

4.3.1 *Estimation of fluid velocity and heat dissipation rate*

55

In addition to the viscosity effect, the local hydraulic losses through the tubing system as well as the heater opposition to fluid flow (heater is inside the tubing system) can cause the efficiency reduction of the MCP. Furthermore, the ferromagnetic nature of the heater supposed a reduction in the total magnetic induction over the fluid. This is due because the magnetic field lines tend to be concentrated no only in the ferrofluid but also in the iron heater, minimizing the induced magnetic field strength over the ferrofluid.

Therefore, accounting for two standard PVC tees, one cooper push-in tee, one push-in PVC elbow and 36cm of tubing as minor hydraulic losses, the velocity of the ferrofluid leaving the system and the amount of heat dissipated for the MCP could be estimated[‡].

$$\Delta P = f \frac{L}{D} \frac{v^2}{2} \tag{4.9}$$

Assuming laminar flow the friction losses (f) can be approximated as $\frac{64}{\text{Re}}$. Therefore, equation (4.9) can be written as:

$$\Delta P = \frac{v64\mu}{2\rho D} \frac{L_e}{D} \tag{4.10}$$

Where for the minor losses $\frac{L_e}{D} = 256$ [24], fluid viscosity $\mu = 83mPa*s$ [5], and D is the tubing internal diameter (*0.00635m*). After some manipulations, the estimated fluid velocity will be: *v= 0.28 cm/s* and the heat dissipation rate can be computed as follows:

$$\dot{q} = \rho v A C p \Delta T$$
$$\dot{q} = 20.07W \tag{4.11}$$

[‡] Calculations performed for the costume water-based ferrite ferrofluid under steady state assumptions.

The maximum amount of power the magnetocaloric pump (MCP) is able to dissipate was finally calculated for the more efficient ferrofluid at optimum operational conditions. For the total 45W of the heater, only a maximum of 8W are used to run the Magnetocaloric Pump; then it is assumed all the heat entering the system is being removed by the ferrofluid. A summary of results and recommendations are presented in the next chapter.

5. CONCLUSIONS AND RECOMMENDATIONS

A more efficient method to produce Mn-Zn ferrites was proposed and the total time for the synthesis reaction was decreased from 5 hours to 1 hour. The amount of ferrite obtained was increased and the ferrofluid production changed from 4ml to 32ml after each synthesis process and the ferrites large-scale production was found to be scalable.

The magnetocaloric energy conversion principle was put in practice and shown to be possible for macro-scale systems. A magnetocaloric pump capable to pump a magnetic fluid using no-moving mechanical parts was designed, characterized by using two different ferrofluids (one water-based and one organic-based) and compared with the simplified Bernoulli equation.

Important parameters of magnetocaloric pumping were identified. The relevance of heat source location in the magnetocaloric energy conversion was tested and an optimum position was recommended. It was found that the inviscid assumption introduce significant errors when a real system is implemented. Ferrofluids synthesized with Mn-Zn ferrites were confirmed to be better for applications near the ambient temperature while the high concentrated ferrofluids show to be poor for the proposed application.

It is recommended the production of $Mn_{0.5}Zn_{0.5}Fe_2O_4$ ferrites in order to obtain a higher pyromagnetic coefficient $\left(\dfrac{\Delta M}{\Delta T} \right)$ and consequently higher magnetocaloric effect. Low viscosity magnetic fluids must be synthesized; thus, a water-based solution it is recommended to obtain a higher MCP response.

APPENDIX A

In order to determine the volumetric fraction and diameter size for the produced water-based Mn-Zn ferrofluid, a magnetic analysis (in addition of X-ray diffraction) was performed. From slope of the curve at low fields the initial susceptibility value (χ_0) is

obtained, while H_0 is obtained from the high field magnetic curve slope and the saturation magnetization value.

High Intensity Magnetic Fields
Costume ferofluid x=0.7

$y = -809102786.05x + 7167.09$
$R^2 = 0.99$
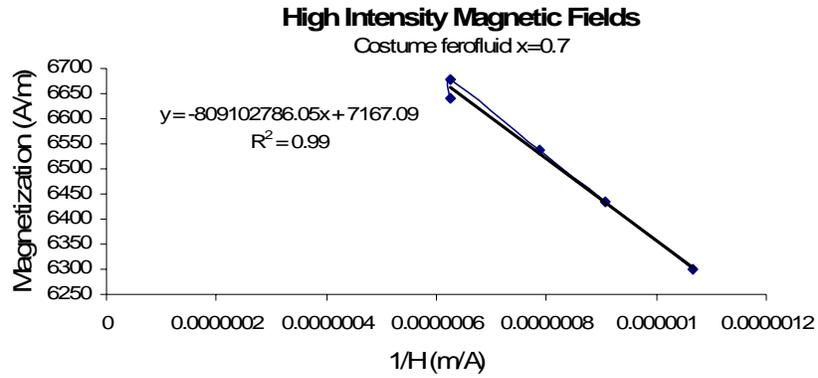
Figure 37: Magnetization curve at high field (H) for produced ferrofluid

Low Intensity Magnetic Fields
Costume ferrofluid x=0.7

$y = 0.1491x$
$R^2 = 0.9981$
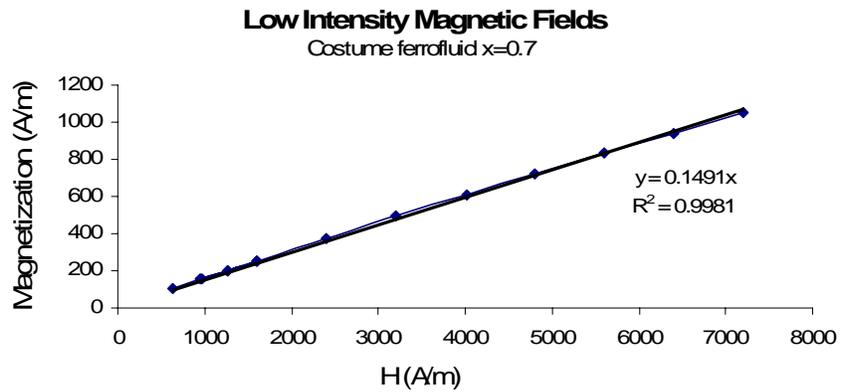
Figure 38: Magnetization curve at low field (H) for produced ferrofluid

Additional results are presented in table 4 section 4.2.1.

APPENDIX B
(Final Magnetocaloric Pump design)

Push-in tee

PVC standard tee

90º Push-in elbow

6 in

Piezometer

Permanent Magnet

Heater

5 in
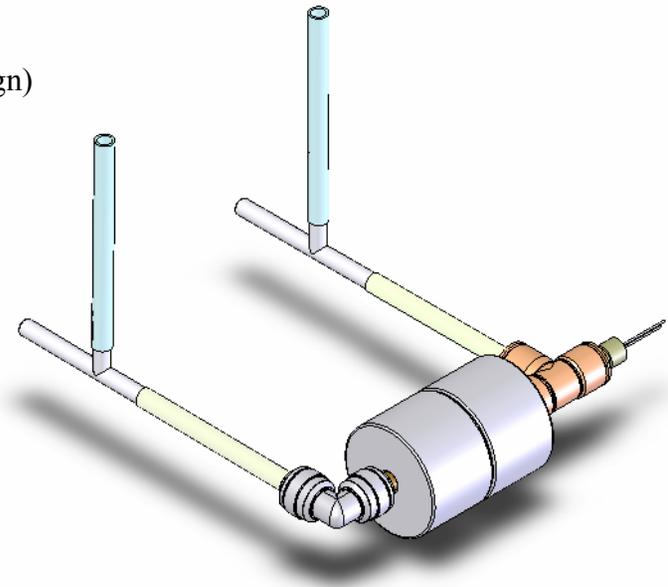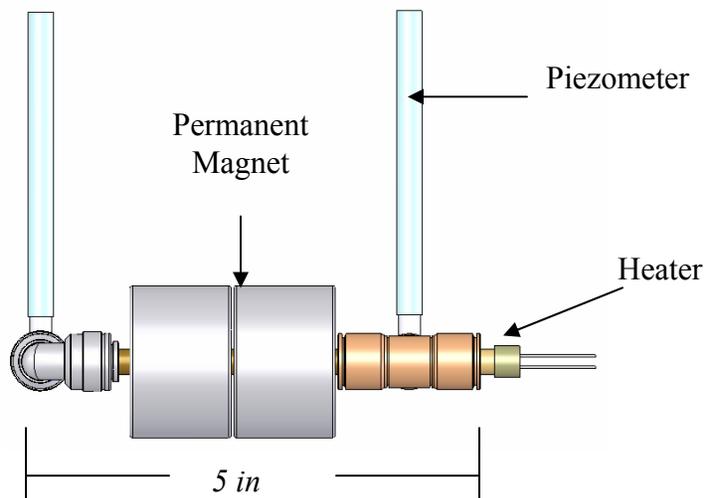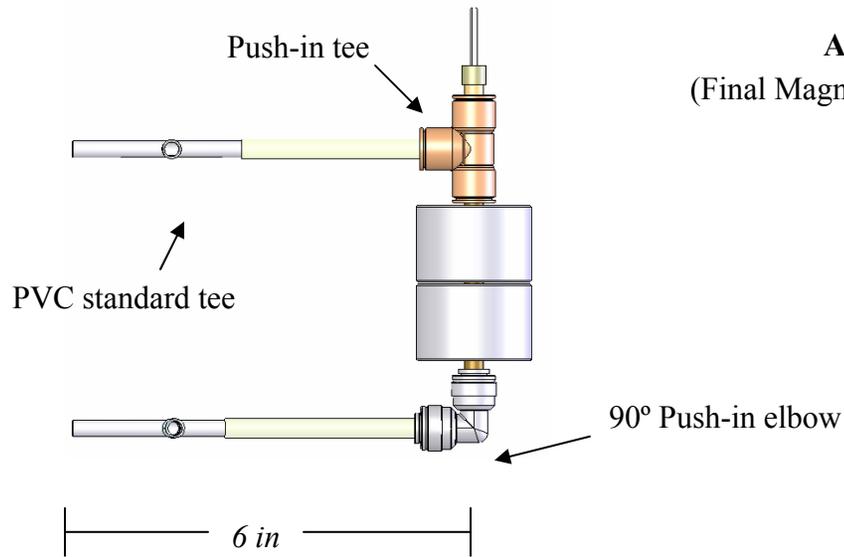
Dwg:			
MAGNETOCALORIC PUMP PROTOTYPE			
By: ERICK O. BERMUDEZ TORRES University of Puerto Rico at Mayaguez			
Item	**Qty**	**Desription**	
90 º Elbow	1	1/4" ID Parker Push-in PVC	
Cooper Tee	1	1/4" Parker Push-in	
Standard tee	2	5/16" OD Standard PVC	
Permanent Magnet	2	0.5Tesla	
Copper tube	1	1/4" ID	
Tubing	1	Clear 40cm High resistant	
Heater	1	1/8" McMaster Cardbridge	

APPENDIX C
(Cross-sectional view of heater location inside the MCP)

A

45W Electrical Heater

1 3/4"

5"

B

90º Push-in PVC elbow

Push-in copper tee

2"

5"

C

Permanent magnet

5 3/4

5"
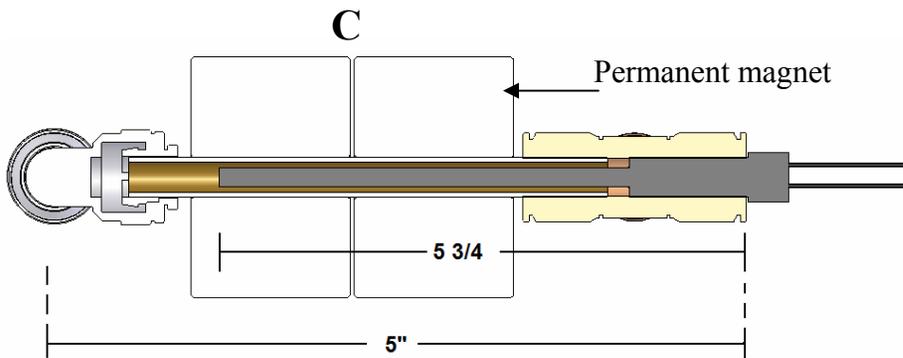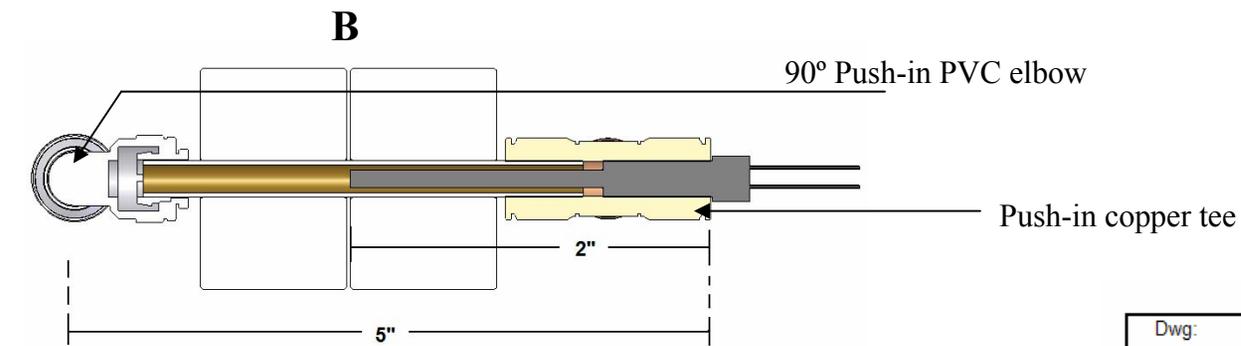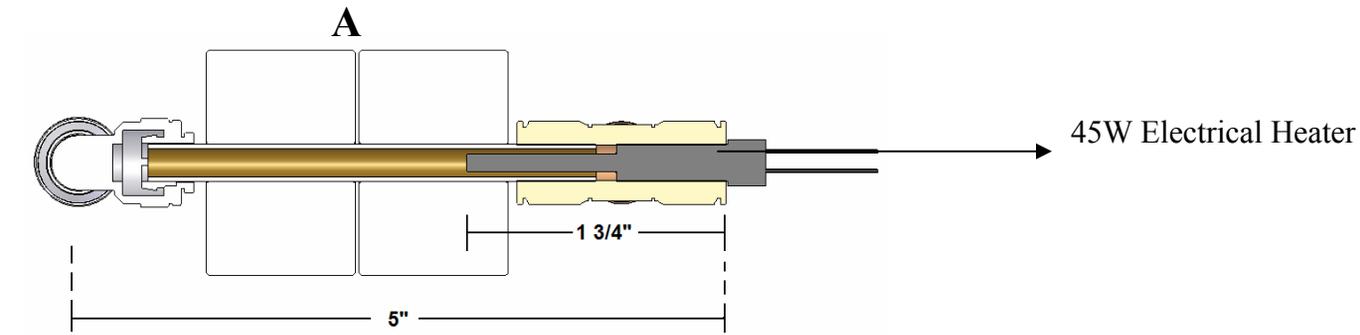
Dwg:		
HEAT SOURCE LOCATION SCHEMATIC		
By: ERICK O. BERMUDEZ TORRES University of Puerto Rico at Mayaguez		
Figure	**Position**	**Desription**
A	Initial	MCP Prototype
B	Medium	MCP Prototype
C	Ending	MCP Prototype

59

REFERENCES

[1] R.E. Rosenweig, Ferrohydro-dynamics, Dover, New York (1997), 1-176

[2] D. Jiles, Introduction to magnetism and magnetic materials, Florida (1998)

[3] R. A Serway, Physics for Scientists and Engineers, James Madison University (1997), 866-891

[4] D. Zins, R. Massart, E. Auzans, E. Blums, Synthesis and Properties of Mn-Zn Ferrite Ferrofluids, Journal of Material Science, 34, 1253-1260, 1999

[5] L.J Love, J.F. Jansen, T.E. Mcknight, Y. Roh, T.J.A Phelps, A Magnetocaloric Pump for Microfluid Applications IEEE Transactions on nanobioscience. Vol 3, No 2, 2004

[6] R. Almurugan, G. Vaidyanatahan, S. Sendhilnatan, B. Jadevayan. Mn-Zn Ferrite nanoparticles for Ferrofluid Preparation: Study on Thermal-Magnetic Properties, Journal of Magnetism and Magnetic Materials, 298 (2006) 83-94

[7]   J.E Cataño, Development of a magnetocaloric pump for heat pipes applications, Mechanical Engineering School, University of Puerto Rico at Mayaguez, MS Thesis, 2005

[8] L, Wang, Z. Fan, A. Roy, and D.E. Laughlin, effects on the atomic ordering on the Curie temperature of FePd $L1_0$ type alloys. Journal of Applied Physics, volume 9, No 11. 2004

[9] E. Calderon, Synthesis and Characterization of Cobalt and Manganese-Zinc Ferrites. Department of Chemistry, University of Puerto Rico at Mayaguez, MS Thesis, 2003

[10] J.E. Cataño, O. Perales, M. Tomar, E. Calderon, And C. Melendez, Characterization of Mn-Zn magnetic fluid for cooling applications at ambient temperature. Technical publication, ASME, Proceedings of IMECE November 2005.

[11] S. Suchi, K. Sacatani and Hi Yamaguchi. An application of a binary mixture of magnetic fluid for heat transport devices. Journal of Magnetism and Magnetic Materials, Vol 272-276 No 3, 2004

[12] V. Lemoff, P. Lee. An AC Magnetohydrodynamic Micropump. Sensors and actuators B 63 (2000) 178-185

[13] J. Zhong, Y. Mingqiang, H. Haim Bau. Magneto Hydrodynamic (MHD) Pump Fabricated with Ceramic tapes Sensors and actuators A 96 (2002) 59-66

[14] R.D.K Misra, S. Gubbala, H. Nathani, K. Koisol, Magnetic Properties of Nanocrysraline Ni-Zn, Zn-Mn, and Ni-Mn Ferrites Synthesis by Reverse Micelle Technique, Journal of Physics 348, 317-328, 2004

[15] P. Podar, H. Srikanth, S.A. Morrison, E.E. Carpenter, Inter-particle Interactions and Magnetism in Manganese-Zinc Ferrite Nanoparticles, Journal of Magnetism and Magnetic Materials, 288 (2005) 443-451

[16] D. Bica and L. Vekas, M. Rasa, Preparation and Magnetic Properties of Concentrated Magnetic Fluids on Alcohol and Water Carrier Liquids Journal of Magnetism and Magnetic Materials, 252 (2002) 10-12

[17] L.M. Pop, C.D. Buioca, V. Iusan, M. Zimnicaru, Long-tern Stability of Magnetic Fluids in Low-gradient Magnetic Fields, Journal of Magnetism and Magnetic Materials, 252 (2002) 46-48

[18] E. Resler, and R. E. Rosensweig, , Regenerative thermomagnetic power, J. Eng. Power, pp. 399-406, 1967.

[19] A. Oakssim, S Fstrea, A. Roch, S. Laurent, Y. Gossuin, C. Piérart, L. Vander Elst, R. N. Muller, Control of the synthesis of magnetic fluid by relaxometry and magnetometry, Journal of Magnetism and Magnetic Materials, 272-276 el1711-e1713, 2004

[20]   R. Muller, R. Hergt, M. Zeisberger, W. Gawalek, Preparation of magnetic nanoparticles with large specific loss power for heating applications, Journal of Magnetism and Magnetic Materials, 2004

[21]   R. Almurugan, G. Vaidyanatahan, S. Sendhilnatan, B. Jadevayan. Effect of Zinc substitution on C0-Zn and Mn-Zn ferrite nanoparticles prepared by co-precipitation, Journal of Magnetism and Magnetic Materials, 288 (2005) 470-477

[22]   R.W Chantrell, J. Popplewell and S.W Charles. Measurements of Particle Size Distribution Parameters in Ferrofluids. IEEE transactions on magnetics, Vol. MAG-14 No. 5, 1978

[23] E. Auzans. Mn-Zn ferrite nanoparticles for water- and hydrocarbon-based ferrofluids: preparation and properties. Institute of Physics of Latvian University. PHD Thesis, 1999.

[24] R. Fox and A. McDonald, Introduction to Fluid Mechanics and engineering approach, 5th Edition, Wiley, pp 347. (2003)